Spring 2017

Forensic research on detecting seam carving in digital images

Jingyu Ye
New Jersey Institute of Technology

Copyright Warning & Restrictions

The copyright law of the United States (Title 17, United States Code) governs the making of photocopies or other reproductions of copyrighted material.

Under certain conditions specified in the law, libraries and archives are authorized to furnish a photocopy or other reproduction. One of these specified conditions is that the photocopy or reproduction is not to be "used for any purpose other than private study, scholarship, or research." If a, user makes a request for, or later uses, a photocopy or reproduction for purposes in excess of "fair use" that user may be liable for copyright infringement,

This institution reserves the right to refuse to accept a copying order if, in its judgment, fulfillment of the order would involve violation of copyright law.

Please Note: The author retains the copyright while the New Jersey Institute of Technology reserves the right to distribute this thesis or dissertation

Printing note: If you do not wish to print this page, then select "Pages from: first page # to: last page #" on the print dialog screen

ABSTRACT

FORENSIC RESEARCH ON DETECTING SEAM CARVING IN DIGITAL IMAGES

by
Jingyu Ye

Digital images have been playing an important role in our daily life for the last several decades. Naturally, image editing technologies have been tremendously developed due to the increasing demands. As a result, digital images can be easily manipulated on a personal computer or even a cellphone for many purposes nowadays, so that the authenticity of digital images becomes an important issue. In this dissertation research, four machine learning based forensic methods are presented to detect one of the popular image editing techniques, called 'seam carving'.

To reveal seam carving applied to uncompressed images from the perspective of energy distribution change, an energy based statistical model is proposed as the first work in this dissertation. Features measured global energy of images, remaining optimal seams, and noise level are extracted from four local derivative pattern (LDP) domains instead of from the original pixel domain to heighten the energy change caused by seam carving. A support vector machine (SVM) based classifier is employed to determine whether an image has been seam carved or not. In the second work, an advanced feature model is presented for seam carving detection by investigating the statistical variation among neighboring pixels. Comprised with three types of statistical features, i.e., LDP features, Markov features, and SPAM features, the powerful feature model significantly improved the state-of-the-art accuracy in detecting low carving rate seam carving. After the feature selection by utilizing SVM based recursive feature elimination (SVM-RFE), with a small

amount of features selected from the proposed model the overall performance is further improved. Combining above mentioned two works, a hybrid feature model is then proposed as the third work to further boost the accuracy in detecting seam carving at low carving rate. The proposed model consists of two sets of features, which capture energy change and neighboring relationship variation respectively, achieves remarkable performance on revealing seam carving, especially low carving rate seam carving, in digital images. Besides these three hand crafted feature models, a deep convolutional neural network is designed for seam carving detection. It is the first work that successfully utilizes deep learning technology to solve this forensic problem. The experimental works demonstrate their much more improved performance in the cases where the amount of seam carving is not serious.

Although these four pieces of work move the seam carving detection ahead substantially, future research works with more advanced statistical model or deep neural network along this line are expected.

FORENSIC RESEARCH ON DETECTING SEAM CARVING IN DIGITAL IMAGES

by
Jingyu Ye

A Dissertation
Submitted to the Faculty of
New Jersey Institute of Technology
in Partial Fulfillment of the Requirements for the Degree of
Doctor of Philosophy in Electrical Engineering

Helen and John C. Hartmann Department of Electrical and Computer Engineering

May 2017

.

APPROVAL PAGE

FORENSIC RESEARCH ON DETECTING SEAM CARVING IN DIGITAL IMAGES

Jingyu Ye

Dr. Yun Q. Shi, Dissertation Advisor — Date
Professor of Electrical and Computer Engineering, NJIT

Dr. Frank Y. Shih, Committee Member — Date
Professor of Computer Science, NJIT

Dr. John D. Carpinelli, Committee Member — Date
Professor of Electrical and Computer Engineering, NJIT

Dr. Sui-Hoi Edwin Hou, Committee Member — Date
Professor of Electrical and Computer Engineering, NJIT

Dr. Xuan Liu, Committee Member — Date
Assistant Professor of Electrical and Computer Engineering, NJIT

BIOGRAPHICAL SKETCH

Author: Jingyu Ye

Degree: Doctor of Philosophy

Date: May 2017

Undergraduate and Graduate Education:

- Doctor of Philosophy in Electrical Engineering,
  New Jersey Institute of Technology, Newark, NJ, 2017

- Master of Science in Electrical Engineering,
  New Jersey Institute of Technology, Newark, NJ, 2009

- Bachelor of Engineering in Electronic Science and Technology,
  Beihang University (BUAA), Beijing, People's Republic of China, 2006

Major: Electrical Engineering

Presentations and Publications:

J. Ye, G. Xu, and Y. Q. Shi, "A deep convolutional neural network for seam carving detection," to be submitted.

J. Ye and Y. Q. Shi, "Deep learning for sharpening detection," to be submitted.

J. Ye and Y. Q. Shi, "A hybrid feature model for detecting seam carving in digital images," to be submitted.

J. Ye and Y. Q. Shi, "An effective method for seam carving detection," *Journal of Inf. Security and Applications*. Accepted.

J. Ye and Y. Q. Shi, "A local derivative pattern based image forensic framework for seam carving detection," *Proc. 15th Int. Workshop Forensics Watermark,* 2016.

J. Wang, T. Li, Y. Q. Shi, S. Lian, and J. Ye, "Forensics feature analysis in quaternion wavelet domain for distinguishing photographic images and computer graphics," *Multimedia Tools and Applications*, 2016.

Z. Zhang, J. Hou, Y. Zhang, J. Ye, and Y. Q. Shi, “Detecting multiple H.264/AVC compressions with same quantization parameters,” *IET Inf. Security*, 2015.

G. Xu, J. Ye, and Y. Q. Shi, “New developments in image tampering detection,” *Proc. 13th Int. Workshop Digital Forensics and Watermarking*, 2014.

Z. Li, J. Ye, and Y. Q. Shi, “Distinguishing computer graphics from photographic images using local binary patterns,” *Proc. 11th Int. Workshop Digital Forensics and Watermarking*, 2012.

P. Sutthiwan, J. Ye, and Y. Q. Shi, “An enhanced statistical approach to identifying photorealistic images,” *Proc. 8th Int. Workshop Digital Forensics and Watermarking*, 2009.

献给我的父亲母亲

ACKNOWLEDGMENT

First and foremost, I would like to express my heartfelt gratitude to my advisor, Dr. Yun-Qing Shi, for his guidance throughout my Ph.D. Without his tremendous assistance and endless encouragement, I could not have completed my dissertation. I am also grateful to my colleagues and friends for their kindly help during my life in NJIT. Finally, I would like to thank my parents for the constant love and support. I could not have done this without you.

TABLE OF CONTENTS

TABLE OF CONTENTS
(Continued)

Chapter **Page**

TABLE OF CONTENTS
(Continued)

LIST OF TABLES

LIST OF FIGURES

LIST OF FIGURES
(Continued)

Figure **Page**

LIST OF FIGURES
(Continued)

Figure **Page**

LIST OF FIGURES
(Continued)

Figure **Page**

CHAPTER 1

INTRODUCTION

1.1 Overview

Due to the efficiency of preserving and exchanging information, digital images have become the most important and influential medium nowadays, thus the authenticity of digital images is crucial to the information security. However, with the tremendous development in digital image editing technology, the integrity of a digital image can no longer be guaranteed because the content of a digital image can be easily manipulated by any individual.

To fight against the counterfeiting and reveal the truth, digital image forensics [1-3] has increasingly attracted wide attention. In the past two decades, remarkable progress has been made on many forensic topics, such as: source identification [4-9], which aims at identifying the acquisition device of an image; copy-move detection [10-14], which is to discover whether an image has duplicated regions; double JPEG compression detection [15-19], which is to detect if an JPEG image has gone through multiple times of JPEG compression; computer graphics classification [20-28], which is to differentiate computer generated graphic images from photographic images.

In this dissertation, the research focuses on detecting seam carving applied to digital images, particularly uncompressed digital images. Traditional image resizing techniques, e.g., interpolation and cropping, can successfully modify the image size. But, the important image content may not be well preserved as shown in Figure 1.1. Therefore, seam carving is proposed to solve this problem. The algorithm of seam carving was firstly invented by

(a)

(b) (c) (d)

Figure 1.1 (a) is a sample image from UCID database. (b), (c) and (d) are resized versions of (a) by using cropping, cubic interpolation and seam carving, respectively. The image size of (a) is 384×512 and 384×359 for each the resized copy.

Avidan and Shamir [29], and the main purpose of the algorithm is to resize an image while preserving the important image content. By successively removing an optimal seam, which is a path of pixels with the lowest accumulative energy, the image can be retargeted to a new size and the visual content can be well preserved. A seam can be horizontal or vertical, i.e., crossing the image from left to right, or from top to bottom, and pixels in a seam are all 8-connected. By forcing each row can only have one pixel be included in a vertical seam, or each column can only have one pixel be included in a horizontal seam, the rectangular shape of the image can be maintained after seam deletion. Because of its content awareness,

seam carving has become one of the most popular image resizing algorithms, and is included as a functionality in many prevalent image editing software, such as Photoshop CS4 and GIMP. Moreover, seam carving can be utilized for image forgery as well, i.e., e.g., for object removal [29]. Although seam carving is one of the most popular image resizing algorithm, the forensic research of seam carving detection is still in the early stage which motivates the works that are to be presented in this dissertation.

1.2 Algorithm of Seam Carving

Seam carving, also known as content-aware image resizing, is such a kind of algorithm aimed at reducing image size without destroying the main content of the image. Its basic idea is to remove multiple seams with lower cumulative energy cost, which can be considered as 'less important' information in the image, from the image to conduct resizing while preserving the image's important content. Each seam is a path consisting of 8-connected pixels either horizontally from left to right, or vertically from top to bottom. Moreover, each horizontal seam can only have one pixel in each column and each vertical seam can only have one pixel in each row. For an $n \times m$ image I, the energy of each pixel can be obtained according to the given energy function e, such as gradient:

$$e\big(I(x,y)\big) = \left|\frac{\partial}{\partial x} I(x,y)\right| + \left|\frac{\partial}{\partial y} I(x,y)\right|. \tag{1.1}$$

Suppose we intend to reduce the width of I, we actually look for vertical seams to delete which are from top to bottom. Each vertical seam is defined as a set of pixels s_i^V:

$$s^V = \{s_i^V\}_{i=1}^n = \{(i, y(i))\}_{i=1}^n, s.t. \forall i, |y(i) - y(i-1)| \leq 1 \quad (1.2)$$

where i is the row coordinate of each involved pixel and $y(i)$ is the column coordinate. Consequently, each vertical seam is 8-connected and only have one pixel in each row. Assume the cumulative energy for each seam is $E(s)$, then the seam s^* with minimum energy is,

$$s^* = \min_s E(s) = \min_s \sum_{i=1}^n e(I(s_i^V)) \quad (1.3)$$

By using dynamic programming, s^* can be determined. The minimum energy M of each pixel (i, j) for all possible connected seams is:

$$M(i,j) = e(i,j) + min\big(M(i-1, j-1), M(i-1, j), M(i-1, j+1)\big). \quad (1.4)$$

With the obtained M matrix, the minimum $M(i, j)$ in the bottom row is the end of the target seam. Then, by backward searching, the entire seam can be tracked. Similarly, the horizontal seams can also be determined. Therefore, after deleting those seams, the image size is reduced and also the important image content is preserved. As shown in Figures 2.2 and 2.3, it is difficult to discriminant if an image, which is resized by seam carving, has been manipulated or not with human eyes.

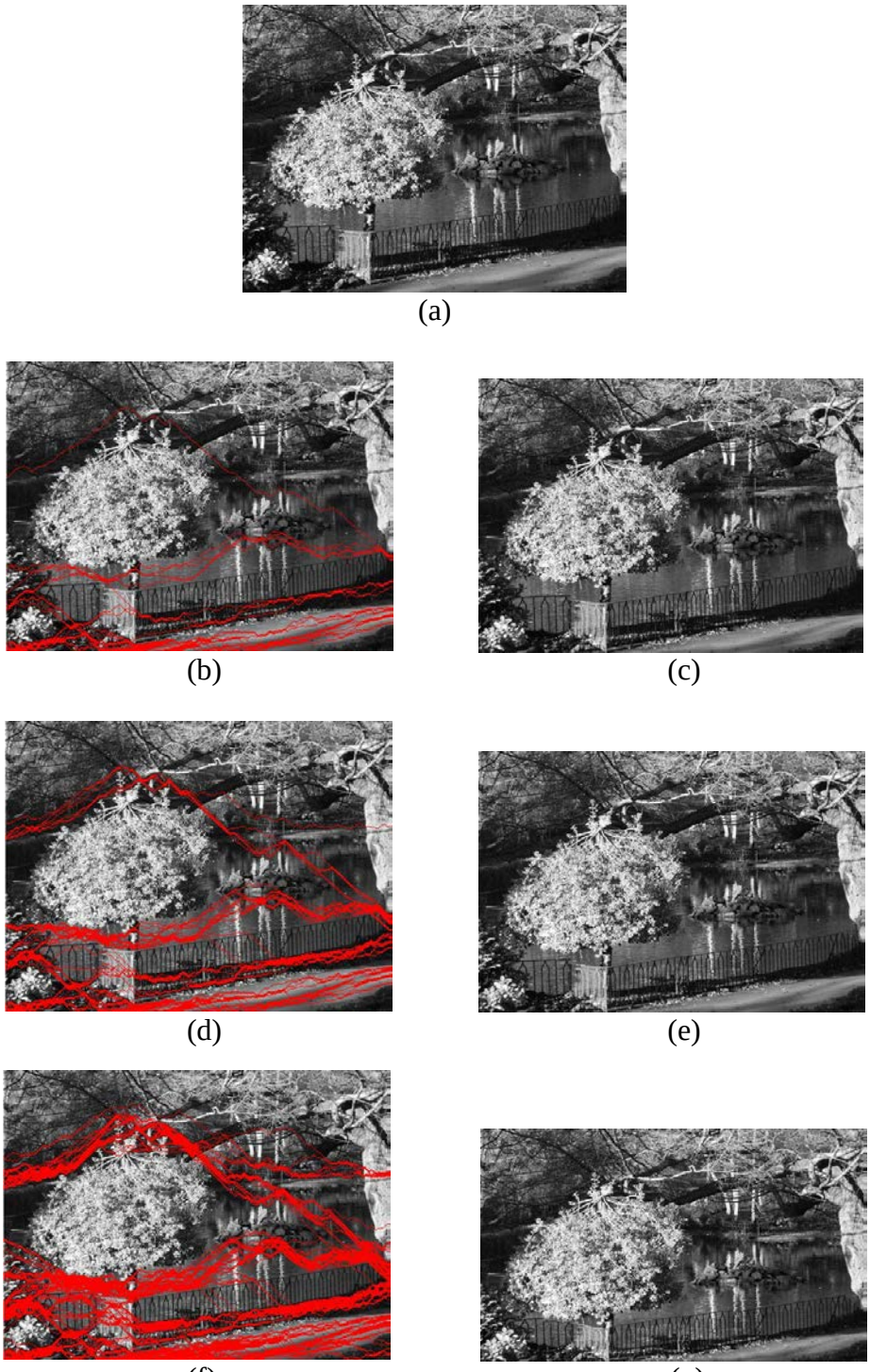

Figure 1.2 (a) An original image from UCID database. Images in (c), (e) and (g) have the same width as (a) but 5%, 10% and 20% less in the height, respectively. The red lines (seams) displayed in (b), (d), and (f) are to be deleted in order to generate the corresponding seam carved copies (c), (e) and (g), respectively.

(a)

(b)

(c)

(d)

(e)

(f)

(g)

Figure 1.3 (a) The same image as shown in Figure2.1 (a). Images in (c), (e) and (g) have the same height as (a) but 5%, 10% and 20% less in the width, respectively. The red lines (seams) displayed in (b), (d), and (f) are to be deleted in order to generate the corresponding seam carved copies (c), (e) and (g), respectively.

1.3 Literature Review

To detect if seam carving has been applied or not, a few works have been presented. Sharker et al. [30] presented the first solution for blind seam carving detection. By modelling the difference JPEG 2-D array with Markov random process [31], the transition probabilities, called Markov features, are utilized to reveal the trace in block-based frequency domain left by the process of seam carving so as to differentiate seam carved JPEG images from un-seam carved ones. Later, Fillion and Sharma [32] proposed a new model comprised of energy bias based features, seam behavior based features and wavelet absolute moments to identify seam carving in uncompressed images.

In [33], Chang et al. tried to discover the artifacts introduced by seam carving applied to JPEG images with blocking artifacts characteristics matrix. As the block misalignment is inevitably occurred due to the deletion of pixels in a JPEG image, seam carved JPEG images and un-seam carved ones could have distinctive DCT blocking artifacts after recompression. Therefore, statistically reviewing the blocking artifacts could be a smart way to distinguish between seam carved JPEG images and non-seam carved JPEG images, which is also indicated from the their reported results. However, the drawback of this method is also obvious because there is no block misalignment problem for the source image which has never gone through JPEG compression. Thus, the performance on detecting seam carving applied to uncompressed images could decrease significantly, as reported in the extended work [34].To also detect seam carved JPEG images, Liu et al. [35] proposed to employ calibrated neighboring joint density and Rich-model based features [36]. This work is then be further improved by [37][38].

In [39], Wei et al. presented an interesting approach for detecting seam carving in uncompressed domain. With the proposed nine types of directional patch operators, 2×2 local region is rebuilt to nine 2×3 predictive patches which represent nine patterns before the possible seam carving process. By comparing the similarity between each predictive patch and the referee patch, the most similar one is considered as the optimal patch and the indexing, which is from zero to eight, is assigned to the given local region. Consequently, an indexing 2-D array is generated in which each element is the indexing of the optimal patch for that particular position. Finally, Markov features extracted from the indexing 2-D array are applied to detect seam carving. Although the state-of-the-art performance was reported, it should be noted that the nine predictive patch operators are designed for detecting the deletion of vertical seams. Therefore, this method could possibly fail on detecting horizontal seam carving.

In Ryu et al.'s work [40], eighteen energy based features, which measure the energy distribution and noise level of a given image, are proposed to unveil the trace of seam carving in uncompressed images. Inspired by this work, the idea was extended by Yin et al. [41]. In Yin et al.'s feature model, eighteen energy features, which are similar to the features presented by Ryu et al., are included. Additionally, another six energy features are proposed to capture the energy variation in half images which results in a twenty-four dimensional feature model. Furthermore, all the proposed features are extracted from the Local Binary Pattern (LBP) [42] encoded images instead of the pixel domain. The reported results indicate the Yin et al.'s method outperforms previously published works.

Besides of the aforementioned machine learning based passive blind forensic methods, an active approach was presented by Lu and Wu [43]. The pre-extracted SIFT

features are encoded and attached to the image at the sender side, and these side information will be thereafter utilized by the receiver to authenticate each received image in order to counter possible seam carving forgery during the transmission. Although this active approach seems effective on detecting seam carving, the limitation is significant since any malicious manipulation made on the side information during the transmission could make it fail. Therefore, this method could work only when a trustworthy communication channel is applicable which could never be true in real world.

1.4 Dissertation Researches

In this dissertation, researches mainly focus on detecting seam carving in uncompressed domain, and four machine learning based passive blind forensic approaches are presented.

To reveal the trace left by the process of seam carving, ninety six energy features are proposed in the first work of this dissertation chapter. By pre-processing the suspicious image with four different LDP operators, four LDP encoded images are obtained from which the proposed ninety six features are extracted. With the SVM based classification, the suspicious image can be identified as either an un-seam carved image or a seam carved image.

Differ from the first model, a pixel variation based feature model, which consists of LDP features, Markov features, and SPAM features, is then presented to capture the change in neighboring pixels so as to detect seam carving. Furthermore, SVM-RFE is applied for feature reduction. Indicated from the experimental results, with a small number of features selected from the feature model, the state-of-the-art performance is achieved.

In the third piece of work, a more advanced feature model is designed based on combining the ideas of previously presented two works to further improve the accuracy of detecting seam carving images with low carving rate, particularly the carving rate as 5% and 10%. According to the conducted experimental works, the state-of-the-art performance has been further improved.

The first deep learning based forensic work on detecting seam carving forgeries is reported as the last piece of work included in this dissertation. The designed deep convolutional neural network which comprises of six convolutional layers has achieved encouraging results on a huge image database. It is believed that such deep learning techniques could be the ultimate solution for this forensic research.

1.5 Outlines

In Chapter 2, an energy based feature model is presented for detecting seam carving in uncompressed images. A pixel variation based feature model comprises of LDP features, Markov features and SPAM features is then proposed in Chapter 3. Chapter 4 introduces a more advanced hybrid feature model in detail. In Chapter 5, a convolutional neural network is designed to determine whether an uncompressed image has gone through the process of seam carving or not. This dissertation is summarized in Chapter 6.

CHAPTER 2

AN ENERGY BASED FEATURE MODEL FOR SEAM CARVING DETECTION

Seam carving is to delete low energy area in a given image, which is considered as less visually important image content, so as to modify image size and preserve more important image content. Therefore, the energy of seam carved image could have difference with the original one, and this change can be utilized for seam carving detection. In [40], 18-D energy based features were proposed to discriminant seam carved images and images without seam carving. Once the image content is removed by seam carving, the distortion will be introduced in the manipulated local area. Consequently, the local descriptor which depicts certain area could also vary compared with before seam carving operation. In [41], the idea of combining local texture pattern and energy based feature was addressed. Then, 24-D energy based features extracted from the LBP encoded image were applied to detect the operation of seam carving. In this chapter, an LDP based forensic framework is proposed as illustrated in Figure 2.1. For each input image, four LDP encoded images are generated and 24-D energy based features are extracted from each LDP image. Consequently, each input image is represented by a 24×4=96-D feature vector. By applying a SVM classifier, a decision of whether the input image is seam carved or not could be made. According to the experimental results, the proposed framework outperforms the prior state of the arts significantly. The framework for detecting seam carving in digital images by utilizing the proposed 96-D feature model is illustrated in Figure 2.1. In the following of this section, the 96-D is introduced in detail.

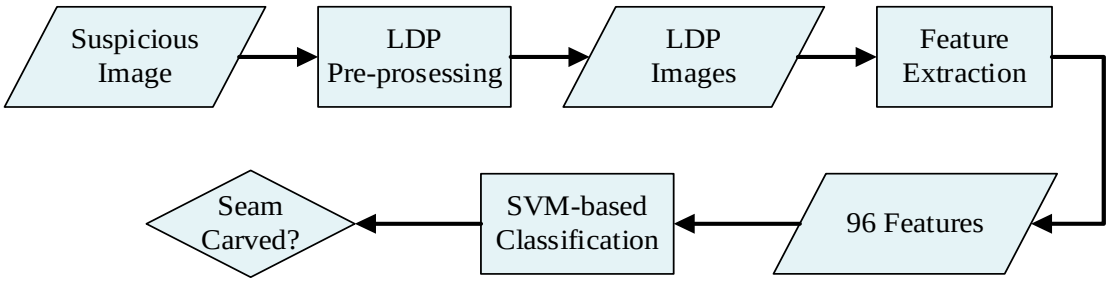

Figure 2.1 Flow chart of forensic investigation with proposed energy based feature model.

2.1 Proposed Energy Based Feature Model

2.1.1 Local Derivative Patterns

As a local descriptor, LDP [44] can be considered as a directional high order derivative binary pattern comparing with LBP which can be considered as the 1st order non-directional descriptor. It captures more discriminate information from the derivative perspective, and more sensitive to the changes of the local region. As shown in Figure 2.2, for a given local 5×5 block with the central pixel at Z_0 in image I, the 1st order derivative of pixel Z_0 in I along the 4 directions $\alpha = 0^o$, 45^o, 90^o and 135^o can be derived as follows,

$$I'_{\alpha=0^o}(Z_0) = I(Z_0) - I(Z_1),$$

$$I'_{\alpha=45^o}(Z_0) = I(Z_0) - I(Z_2),$$

$$I'_{\alpha=90^o}(Z_0) = I(Z_0) - I(Z_3),$$

$$I'_{\alpha=135^o}(Z_0) = I(Z_0) - I(Z_4) \quad (2.1)$$

$I(Z_{15})$	$I(Z_{14})$	$I(Z_{13})$	$I(Z_{12})$	$I(Z_{11})$
$I(Z_{16})$	$I(Z_4)$	$I(Z_3)$	$I(Z_2)$	$I(Z_{10})$
$I(Z_{17})$	$I(Z_5)$	$I(Z_0)$	$I(Z_1)$	$I(Z_9)$
$I(Z_{18})$	$I(Z_6)$	$I(Z_7)$	$I(Z_8)$	$I(Z_{24})$
$I(Z_{19})$	$I(Z_{20})$	$I(Z_{21})$	$I(Z_{22})$	$I(Z_{23})$

Figure 2.2 Local 5×5 block with central pixel at Z_0 in image *I*.

where $I(Z)$ is the intensity of pixel *Z*. Considering pixels $\{Z_i | i = 1 \dots 8\}$ which are adjacent to Z_0 with a distance equal to 1 pixel, the 2nd order LDP of Z_0 can be encoded by,

$$LDP_\alpha^2(Z_0) = \{f(I'_\alpha(Z_0), I'_\alpha(Z_1)), \quad \dots, f(I'_\alpha(Z_0), I'_\alpha(Z_8))\} \tag{2.2}$$

where $f(\cdot,\cdot)$ is a binary coding function. It encodes the co-occurrence of neighboring derivative directions with the following rule,

$$f(I'_\alpha(Z_0), I'_\alpha(Z_i)) = \begin{cases} 0, if\ I'_\alpha(Z_0) \cdot I'_\alpha(Z_i) > 0 \\ 1, otherwise \end{cases}, i = 1 \dots 8. \tag{2.3}$$

By doing so, each pixel is encoded and can be represented by its LDP_α^2 along direction α, which is an 8-bit binary number. With the function as below,

$$DLDP_\alpha^2(Z_0) = \sum_{i=1}^{8} f(I'_\alpha(Z_0), I'_\alpha(Z_i)) \cdot 2^{i-1} - 1, \tag{2.4}$$

LDP_{α}^{2} is then converted to a decimal number, denoted as $DLDP_{\alpha}^{2}$, within the range of [0, 255]. Consequently, the $DLDP_{\alpha}^{2}$ 2D-array, called *LDP* image in this work, is generated for the original image. As illustrated in Figure 2.3, $LDP_{0^o}^{2}$ of the central pixel $I(Z_0) = 40$ in a selected 5×5 region is $\{00001100\}$, and the corresponding $DLDP_{0^o}^{2}(Z_0)$ is calculated as 48. By decimalizing the $LDP_{0^o}^{2}$ for each pixel, the generated $DLDP_{0^o}^{2}$ 2D-array is visualized as shown in Figure 2.3. Since LDP is derivative based as indicated by Equation 2.1, which is the intensity difference of each pair of pixels, LDP could be easily changed during the operation of seam carving thus more sensitive to seam carving than LBP, which directly applies the pixel intensity value. Therefore, it is expected that the LDP image contains more discriminative information than the LBP image, which has been verified in the experimental works. As seams are always removed from the images horizontally or vertically by the process of seam carving, we adopted horizontal and vertical *DLDP* in this work.

By applying multi-resolution [45] of LDP, we can not only monitor the changes at adjacent locations but also monitor the changes at the locations with certain distance. For example, the central pixels and eight neighboring pixels are shown in Figures 2.4 (a) and (b) when D is set to 1 or 2, respectively. Moreover, the circular sampling is utilized instead of the rectangular sampling because rectangular sampling could cause information loss when the number of sampled pixels is less than the total number of pixels in the local area. As shown in Figure 2.4 (b), the information of the eight unselected neighboring pixels with D = 2 are lost in the calculation of central pixel's LDP. However, those information could

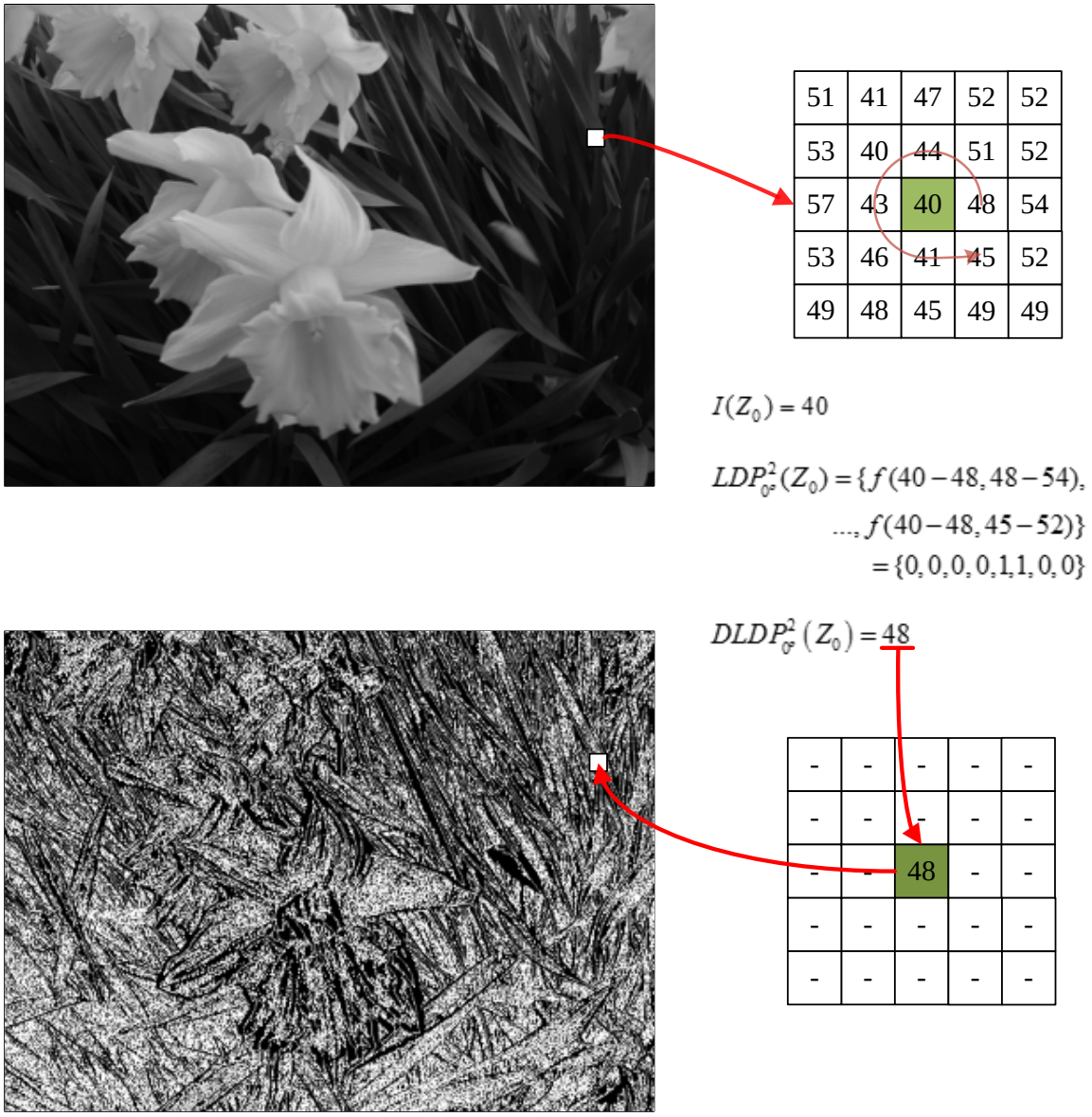

Figure 2.3 Example of the calculation of DLDP for central pixel at Z_0 in a local 5×5 block of image I.

be covered by circular sampling since the pixels not necessarily in the center of each box are interpolated by adjacent four pixels as shown in Figure 2.4 (d). Therefore, based on these considerations, discussed above, it is proposed to use the LDP images generated by the 2nd order LDP with radius equal to 1 and 2, $\alpha = 0^o$ and 90^o, respectively. As shown in

Figure 2.5, four LDP images are visually distinct from each other, because each of them depicts a particular relationship between pixels in the original image. And thus, it is believed that the information carried by these LDP images are complementary and can lead to a better performance than any individual. This expectation has been verified by the experimental works reported in Section 2.3.

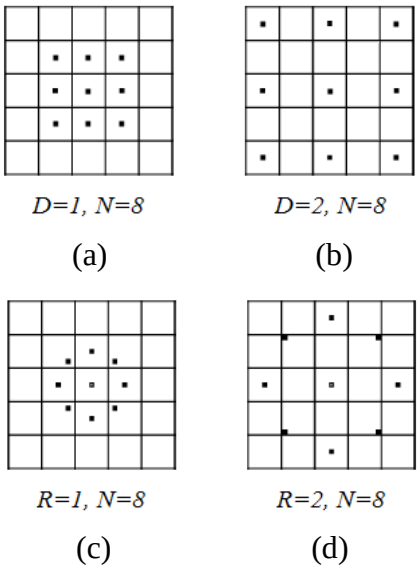

Figure 2.4 (a) and (b) are the 8 rectangular symmetric neighbors with distance, denoted as *D*, equal to 1 and 2, respectively; (c) and (d) are the 8 circular symmetric neighbors with radius, denoted as *R*, equal to 1 and 2, respectively. *N* is the number of sampled neighbors.

(a) Original image

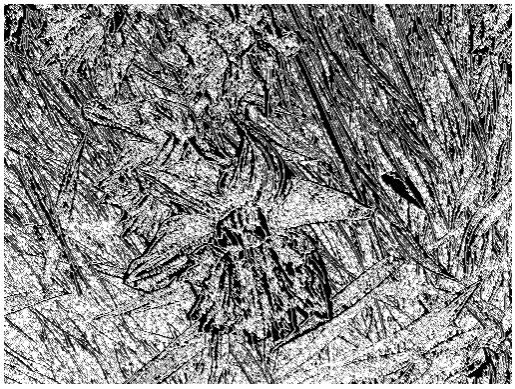

(b) LDP image, R = 1, $\alpha = 0^o$

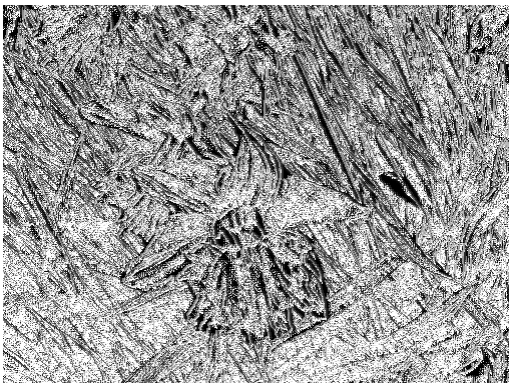

(c) LDP image, R = 2, $\alpha = 0^o$

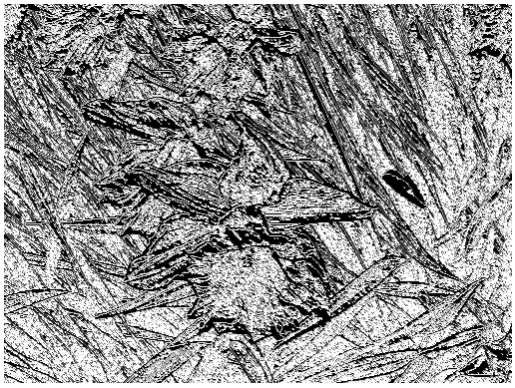

(d) LDP image, R = 1, $\alpha = 90^o$

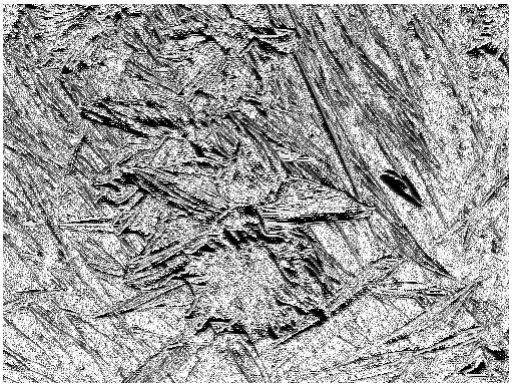

(e) LDP image, R = 2, $\alpha = 90^o$

Figure 2.5 Sample image (a) from UCID and its four LDP encoded images (b), (c), (d), and (e).

2.1.2 Energy Based Features

As seam carving is to remove low energy seams so as to manipulate the image size, it is expected that the energy distribution of an un-touched (not seam carved) uncompressed digital image and its seam carved copy are different. Therefore, features measuring the energy of an image could be used to detect the traces of seam carving. As reported in both [40][41], the energy based feature model has been shown its effectiveness on unveiling the process of seam carving, and particularly indicated in [41] that energy features extracted from LBP domain is more discriminant than the features extracted from pixel domain. Inspired by these two pieces of work, we kept the 24 energy features and extended to totally 96 features to detect seam carved images. The proposed 96 features consist of four groups of 24 features where each group of 24 features is extracted from one of the four LDP images introduced in Section 2.2.1. In the following, a group of the 24 features will be introduced.

Considering that the global energy distribution is changed because of the deletion of low energy pixels, four average energy based features, i.e., average horizontal energy, average vertical energy, the summation and the difference of the former two features, are extracted to differentiate the seam carved images from the un-touched images. Besides, since each optimal seam which has the lowest accumulative energy will be deleted by the seam carving, the energy of the remaining seams will be different. Thus, sixteen seam energy based features are extracted to capture changes of seams energy during the seam carving. By constructing the M matrix in Equation 1.4, the minimum cumulative energy matrix, for each image where the bottom row is the energy of each possible vertical seam, five statistic values called min, max, mean, standard deviation, and the difference between min and max are applied as the features. Also, the other five features of horizontal seams

are calculated accordingly as well. Furthermore, with the M matrix generated by half of the image, six half-seam energy features including min, max and mean for both horizontal seams and vertical seams can be derived similarly.

Furthermore, because the image content has been manipulated by the seam carving, the noise level of the seam carved image could be differed from the original image. To obtain the noise residue *N* of each image *I*, the Wiener filter with 5×5 window, denoted as *F*, is applied to generate the de-noised copy and the noise residue can be derived by,

$$N = I - F(I). \tag{2.5}$$

Then, the mean, standard deviation, skewness and kurtosis of the noise residue are extracted as the features for detecting seam carving. Consequently, for each of the four LDP image aforementioned, 24 features can be obtained, as summarized in Tables 2.1, 2.2, and 2.3. Therefore, the total 96 features are utilized for the classification of seam carving.

Table 2.1 Description of 24 Energy Features

Feature	Description
1. Average Horizontal Energy	$\frac{1}{m \times n}\sum_{i=1}^{m}\sum_{j=1}^{n}\left\|\frac{\partial}{\partial x}I(i,j)\right\|$
2. Average Vertical Energy	$\frac{1}{m \times n}\sum_{i=1}^{m}\sum_{j=1}^{n}\left\|\frac{\partial}{\partial y}I(i,j)\right\|$
3. Sum of Feature #1 and #2	$\frac{1}{m \times n}\sum_{i=1}^{m}\sum_{j=1}^{n}\left(\left\|\frac{\partial}{\partial x}I(i,j)\right\| + \left\|\frac{\partial}{\partial y}I(i,j)\right\|\right)$
4. Difference of Feature #1 and #2	$\frac{1}{m \times n}\sum_{i=1}^{m}\sum_{j=1}^{n}\left(\left\|\frac{\partial}{\partial x}I(i,j)\right\| - \left\|\frac{\partial}{\partial y}I(i,j)\right\|\right)$

Table 2.2 Description of 24 Energy Features (Continued)

Feature	Description
5. Horizontal $Seam_{max}$	$max_{i=1}^{m} M(i,n)$
6. Horizontal $Seam_{min}$	$min_{i=1}^{m} M(i,n)$
7. Horizontal $Seam_{mean}$	$\frac{1}{m}\sum_{i=1}^{m} M(i,n)$
8. Horizontal $Seam_{std}$	$\sqrt{\frac{1}{m}\sum_{i=1}^{m}(Horizontal\ Seam_{mean} - M(i,n))^2}$
9. Horizontal $Seam_{diff}$	$Horizontal\ Seam_{max} - Horizontal\ Seam_{min}$
10. Vertical $Seam_{max}$	$max_{i=1}^{n} M(m,i)$
11. Vertical $Seam_{min}$	$min_{i=1}^{n} M(m,i)$
12. Vertical $Seam_{mean}$	$\frac{1}{n}\sum_{i=1}^{n} M(m,i)$
13. Vertical $Seam_{std}$	$\sqrt{\frac{1}{n}\sum_{i=1}^{n}(Vertical\ Seam_{mean} - M(m,i))^2}$
14. Vertical $Seam_{diff}$	$Vertical\ Seam_{max} - Vertical\ Seam_{min}$

Table 2.3 Description of 24 Energy Features (Continued)

Feature	Description
15. Half-Horizontal Seam$_{max}$	$max_{i=1}^{m} M(i, \frac{n}{2})$
16. Half-Horizontal Seam$_{min}$	$min_{i=1}^{m} M(i, \frac{n}{2})$
17. Half-Horizontal Seam$_{mean}$	$\frac{1}{m}\sum_{i=1}^{m} M(i, \frac{n}{2})$
18. Half-Vertical Seam$_{max}$	$max_{i=1}^{n} M(\frac{m}{2}, i)$
19. Half-Vertical Seam$_{min}$	$min_{i=1}^{n} M(\frac{m}{2}, i)$
20. Half-Vertical Seam$_{mean}$	$\frac{1}{n}\sum_{i=1}^{n} M(\frac{m}{2}, i)$
21. Noise$_{mean}$	$\frac{1}{m \times n}\sum_{i=1}^{m}\sum_{j=1}^{n} N(i,j)$
22. Noise$_{std}$	$\sqrt{\frac{1}{m \times n}\sum_{i=1}^{m}\sum_{j=1}^{n} (N(i,j) - Noise_{mean})^2}$
23. Noise$_{skewness}$	$\frac{1}{m \times n}\sum_{i=1}^{m}\sum_{j=1}^{n} (\frac{N(i,j) - Noise_{mean}}{Noise_{std}})^3$
24. Noise$_{kurtosis}$	$\frac{1}{m \times n}\sum_{i=1}^{m}\sum_{j=1}^{n} (\frac{N(i,j) - Noise_{mean}}{Noise_{std}})^4$

2.2 Experimental Results

In this section, we first introduce the establishment of image database which are utilized to evaluate the proposed method. Then, a comprehensive series of experiments based on Matlab are introduced, and finally the results are reported and compared with the state-of-the-art.

2.2.1 Setup of Seam Carving Database

To evaluate the performance of the proposed method, the seam carved image database has been established on the UCID (Uncompressed Colorful Image database) [47], a popular benchmark database used on image forensics researches which consisting of 1338 uncompressed color images. All the color images have been converted to grayscale images and formed the un-seam carved image set. Seam carving technique proposed in [30] was implemented in MATLAB to produce seam carved images. The image gradient computed by the Sobel operator [48] was applied as the energy function used in Equation 1.1. Then, for each image of the un-seam carved image set, 12 different seam carved copies were generated according to various carving rates, i.e., 5%, 10%, 20%, 30%, 40% and 50%, and two carving directions, i.e., horizontal and vertical. The carving rate C% means, seams are horizontally or vertically carved in order to reduce the size by C%. The ‘H’ and ‘V’ labeled after the C% represent the horizontal carving and vertical carving, respectively. For instance, ‘5%H’ image set contains the seam carved image whose size has been reduced by 5% with horizontal seam deletion. As a result, 12 different seam carved image sets were generated, and each set has 1338 images with same carving rate and carving direction. In other words, 12 seam carving cases were investigated in the experiments. To test on each seam caving scenario, the un-seam carved image set and one of the 12 seam carved image

sets are selected to form the experimental image database. Then, in order to validate the performance, each reported result is the average detection accuracy over 10 iterations of 6-fold cross validation. To build the support vector machine (SVM) classifiers, Lib-SVM library [46] was utilized in the experiments and linear kernel with default parameters was selected.

2.2.2 Performance of Proposed Framework

In order to evaluate the performance of the proposed framework, the experimental works have been conducted on the pre-built 12 different seam carving datasets. Meanwhile, the approaches presented by Ryu et al. [40] and Yin et al. [41], which represent the state-of-the-art, have been implemented and tested to make a fair comparison. As shown in Figure 2.6, the proposed method outperforms the two approaches on all 12 seam carving scenarios. Receiver operating characteristic (ROC) curves of all three compared methods on detecting seam carving at carving rate as 5%, 10%, and 20% are shown in Figures 2.7, 2.8, and 2.9, respectively. And from Table 2.4, it is easy to observe that the average detection accuracies achieved by the proposed framework are significantly higher than that achieved by the other two compared methods. Especially on the low carving rate cases, i.e., 5%, 10% and 20%, the proposed method can achieve 5%-10% higher classification rates than that by the state of the arts, respectively.

Table 2.4 Average Detection Accuracy of Proposed 96-D Model versus the State-of-the-Art

	5%	10%	20%	30%	40%	50%
Ryu et al. (2014)	65.89%	75.15%	85.79%	92.11%	95.26%	97.25%
Yin et al. (2015)	58.72%	70.22%	87.37%	95.63%	98.58%	99.51%
Proposed 96-D	**73.03%**	**88.88%**	**97.78%**	**99.44%**	**99.91%**	**99.96%**

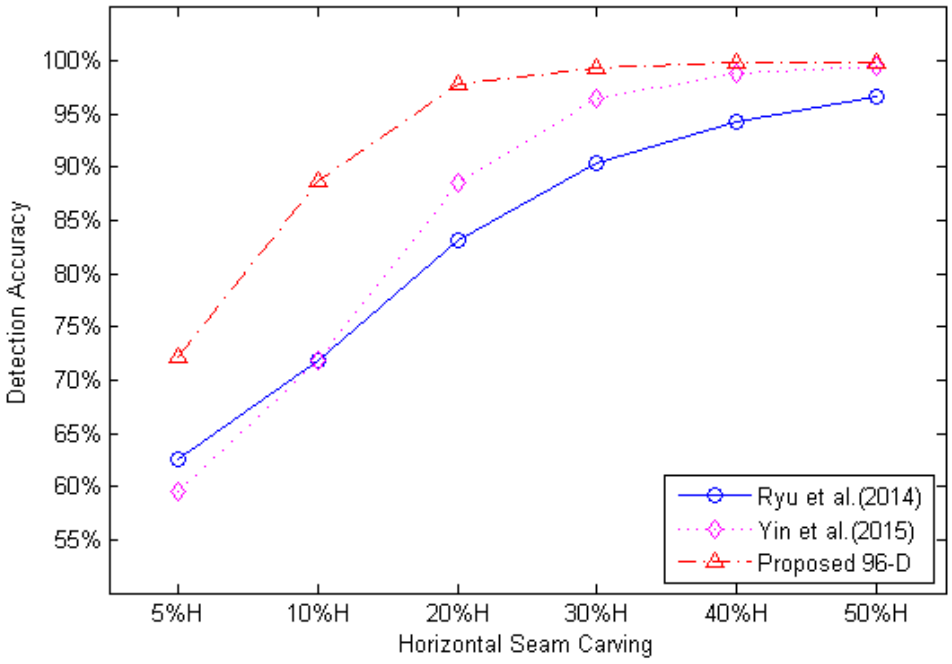

(a)

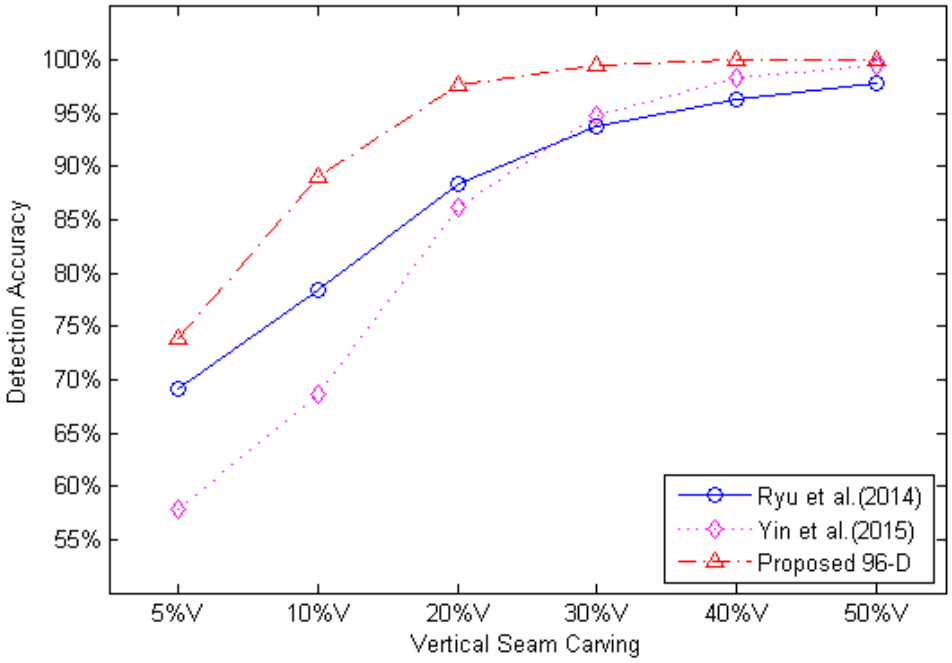

(b)

Figure 2.6 Performance of proposed 96-D model versus the state-of-the-art on detecting 12 different seam carving scenarios.

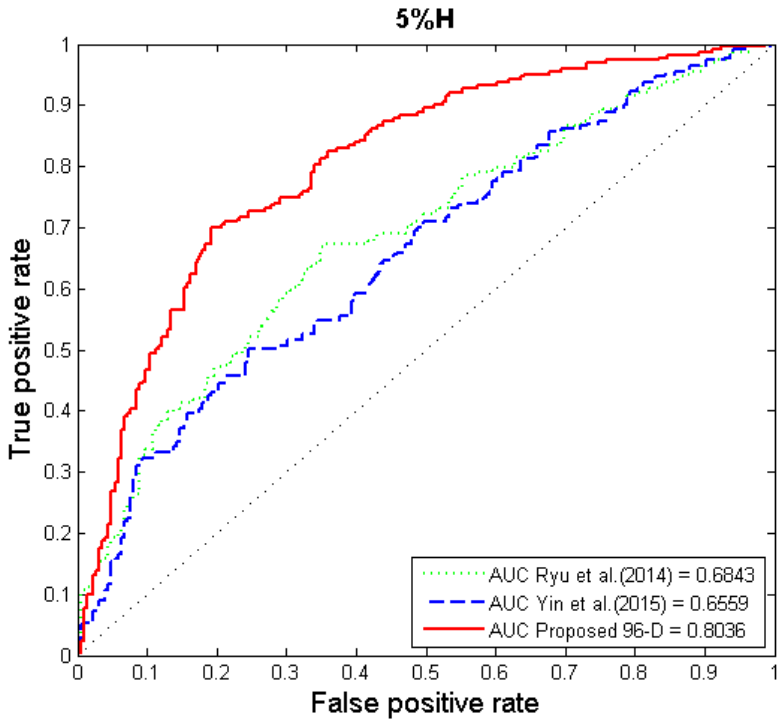

(a)

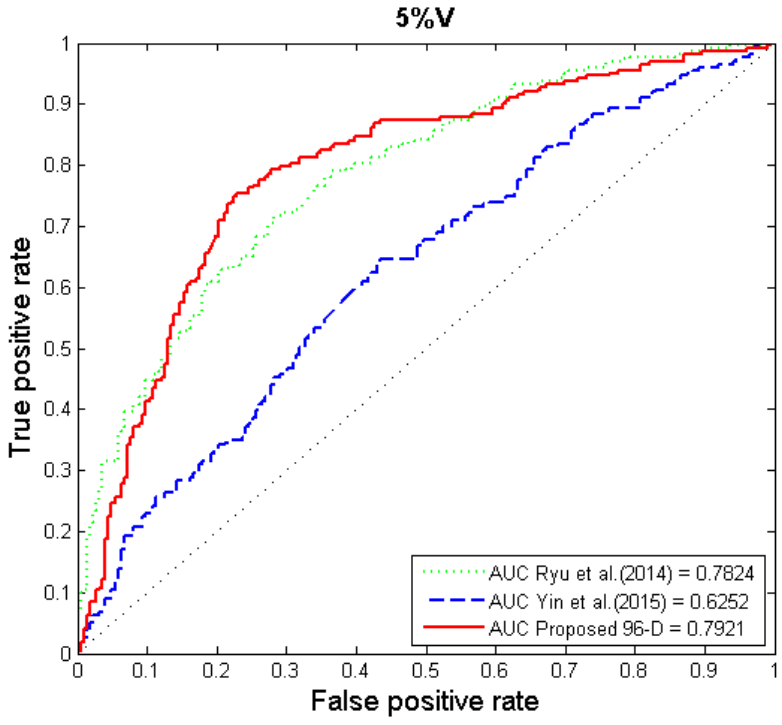

(b)

Figure 2.7 ROCs of three compared methods on detecting seam carving at a carving rate as 5%.

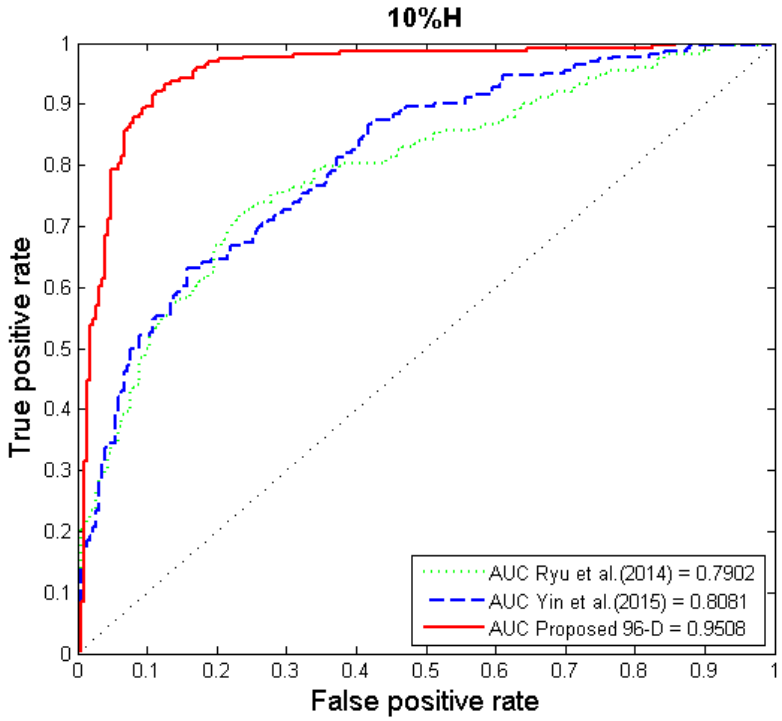

(a)

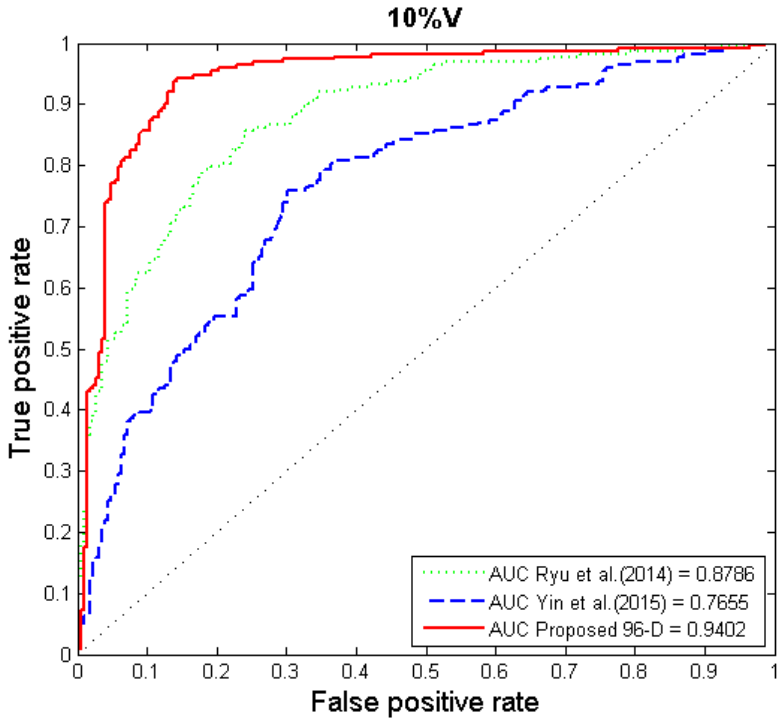

(b)

Figure 2.8 ROCs of three compared methods on detecting seam carving at a carving rate as 10%.

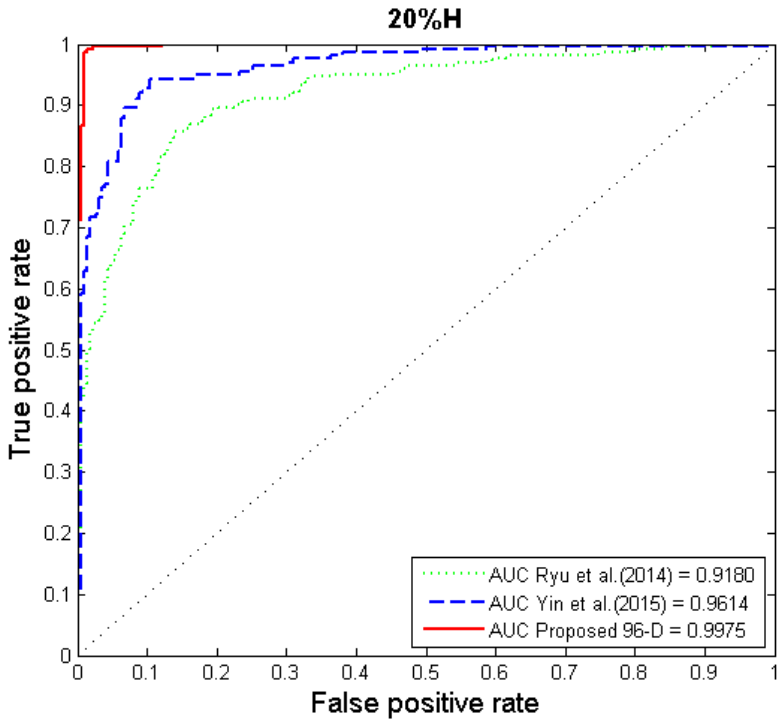

(a)

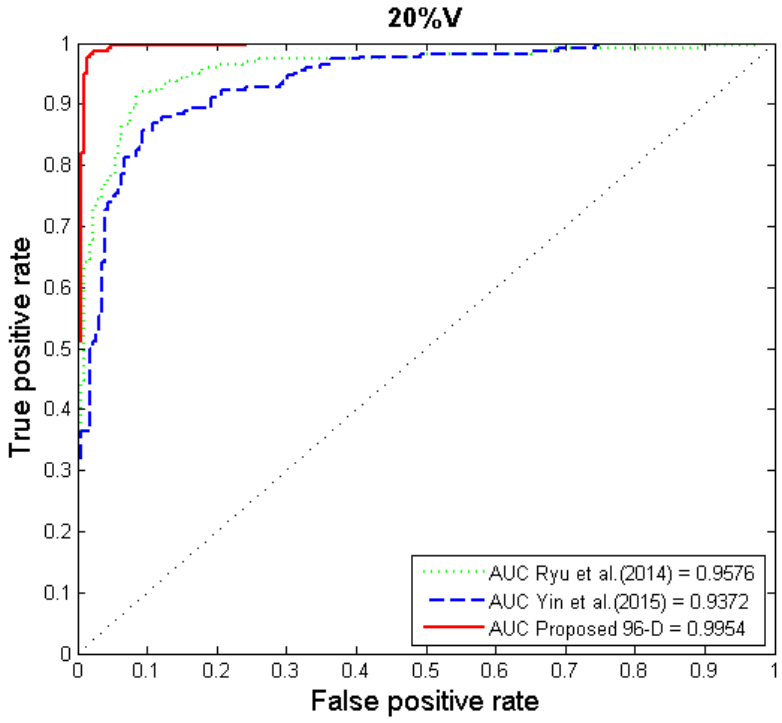

(b)

Figure 2.9 ROCs of three compared methods on detecting seam carving at a carving rate as 20%.

The contribution of each LDP image has also been evaluated. Each group of 24-D features extracted from each LDP image has been tested on the 12 seam carving scenarios respectively, and the test results are reported in Table 2.5. In Table 2.5, the first column stands for each LDP image. The 'h1' is the LDP image 1 as shown in Fig. 3 which is encoded by LDP operator with $\alpha = 0^o$ and radius R = 1; the 'h2' is the image encoded with $\alpha = 0^o$ and R = 2. Similarly, 'v1' and 'v2' are the images encoded by LDP operator with $\alpha = 90^o$ and radius equal to 1 and 2, respectively. It can be observed that the individual performance of the features extracted from each LDP image is much lower than the performance achieved when all features are combined even though the individual performance is not bad at all. This demonstrates that the information carried by each LDP image are complementary and it supports our previous assumption.

Table 2.5 Detection Accuracy of Features Extracted from each LDP Image

	5%H	10%H	20%H	30%H	40%H	50%H
h1	65.38%	77.96%	93.28%	98.06%	99.25%	99.61%
h2	65.12%	80.46%	93.91%	98.20%	99.23%	99.72%
v1	62.35%	77.95%	92.44%	98.15%	99.47%	99.76%
v2	63.39%	80.83%	94.78%	98.51%	99.50%	99.90%

	5%V	10%V	20%V	30%V	40%V	50%V
h1	65.06%	80.74%	93.79%	98.58%	99.73%	100.00%
h2	67.17%	82.94%	95.35%	98.61%	99.93%	100.00%
v1	62.25%	76.84%	91.89%	96.98%	98.85%	99.66%
v2	62.16%	80.19%	94.62%	98.40%	99.32%	99.89%

To further test the performance of the proposed framework, another test on a mixed seam carving image set has been conducted. By randomly selecting 1/12 samples from each of the 12 different seam carved image sets previously established, while each sample is generated from different original image, the mixed seam carving image set is formed.

Then, the proposed framework has been tested on this mixed set and a more than 90% detection accuracy is achieved while the best result achieved by the three compared approaches is only 86%, which was achieved by [41].

2.3 Conclusion

In this chapter, a LDP based image forensic framework is presented for detecting the operation of seam carving. By converting a given image to four LDP encoded images, 96 energy based features are extracted to discriminate if the image is seam carved or un-touched. According to the experimental results, the proposed method can successfully detect seam carving and outperform the state-of-the-art on the various seam carving scenarios. In particular, the proposed framework has achieved 72%, 88% and 97% average detection accuracies on low carving rate cases, i.e., 5%, 10% and 20%, respectively, which is 5%-10% higher than the performance achieved by the previous state of the arts. And the test results on the mixed test sets also indicate the proposed method is more robust than the state-of-the-art.

CHAPTER 3

A PIXEL VARIATION BASED STATISTICAL MODEL FOR SEAM CARVING DETECTION

As presented in Chapter 2, energy based features are proposed to reveal the process of seam carving. In this chapter, a more advanced feature model which statistically depicts changes made among neighboring pixels is presented to unveil the trace of seam carving. In the proposed feature model, each image is represented by a feature vector which consists of LDP features, Markov features, and SPAM features. As LDP encodes the local derivative information with an 8-bit binary pattern, the relation between the central pixel and its eight neighboring pixels depicted by LDP is more complicated than other low-order local descriptors such as LBP. In other words, LDP is more sensitive to the manipulation of the local area, including the pixels that are deleted by seam carving.

Both the Markov transition probability, denoted as Markov features, and the subtractive pixel adjacency model, denoted as SPAM features, are transition probability based. The difference between the Markov features and the SPAM features is mainly on the order, because Markov feature depicts the relation between two adjacent pixels while SPAM feature normally represents the relation between three or more consecutive adjacent pixels. As the pixels with lower energy may be deleted by seam carving, the distribution of pixel values will be changed too and so as the transition probability. Therefore, Markov features and SPAM features could also be sensitive to the seam carving process.

In summary, all of these three types of features can capture the changed relation between neighboring pixels, and it is believed that the combination could be more

discriminative. Thus, we proposed this advanced feature model for the seam carving detection. To further improve the performance of the proposed feature model, SVM-recursive feature elimination has been employed for feature selection. In what follows, the proposed advanced statistical feature model and the feature selection scheme are introduced in detail.

3.1 Proposed Feature Model

3.1.1 Local Derivative Pattern Features

As introduced in Subsection 2.1.1, each binary bit of LDP depicts the relationship of at least three pixels, which is differ from the lower order local descriptor such as LBP that reveals the relation of only two neighboring pixels. For instance, the first order derivatives at pixels Z_0 and Z_4, as shown in Figure 3.1, along $\alpha = 0^o$ are $I'_{0^o}(Z_0)$ and $I'_{0^o}(Z_4)$ respectively, where $I'_{0^o}(Z_0)$ is calculated from Z_0 and Z_4, and $I'_{0^o}(Z_4)$ is derived from Z_4 and Z_{15}. If Z_4 is deleted by seam carving, Z_{15} and the pixels on the right side of Z_{15} in the same row will be shifted to the left by one pixel. The binary bit $f(I'_{0^o}(Z_0), I'_{0^o}(Z_4))$ of $LDP^2_{0^o}(Z_0)$ will be replaced by $f\left(I'^{\Delta}_{0^o}(Z_0), I'_{0^o}(Z_{15})\right)$, where $I'^{\Delta}_{0^o}(Z_0) = I(Z_0) - I(Z_{15})$.

$I(Z_{10})$	$I(Z_{11})$	$I(Z_{12})$	$I(Z_{13})$	$I(Z_{14})$
$I(Z_{25})$	$I(Z_1)$	$I(Z_2)$	$I(Z_3)$	$I(Z_{15})$
$I(Z_{24})$	$I(Z_9)$	$I(Z_0)$	$I(Z_4)$	$I(Z_{16})$
$I(Z_{23})$	$I(Z_8)$	$I(Z_6)$	$I(Z_5)$	$I(Z_{17})$
$I(Z_{22})$	$I(Z_{21})$	$I(Z_{20})$	$I(Z_{19})$	$I(Z_{18})$

$I'_\alpha(Z_{10})$	$I'_\alpha(Z_{11})$	$I'_\alpha(Z_{12})$	$I'_\alpha(Z_{13})$	$I'_\alpha(Z_{14})$
$I'_\alpha(Z_{25})$	$I'_\alpha(Z_1)$	$I'_\alpha(Z_2)$	$I'_\alpha(Z_3)$	$I'_\alpha(Z_{15})$
$I'_\alpha(Z_{24})$	$I'_\alpha(Z_9)$	$I'_\alpha(Z_0)$	$I'_\alpha(Z_4)$	$I'_\alpha(Z_{16})$
$I'_\alpha(Z_{23})$	$I'_\alpha(Z_8)$	$I'_\alpha(Z_6)$	$I'_\alpha(Z_5)$	$I'_\alpha(Z_{17})$
$I'_\alpha(Z_{22})$	$I'_\alpha(Z_{21})$	$I'_\alpha(Z_{20})$	$I'_\alpha(Z_{19})$	$I'_\alpha(Z_{18})$

Figure 3.1 Local 5×5 block with central pixel at Z_0 in image I and the resulting 5×5 derivatives block.

Only if $sign(I_{0^o}^{\prime\Delta}(Z_0) \cdot I_{0^o}^{\prime}(Z_{15}))$ is equal to $sign(I_{0^o}^{\prime}(Z_0) \cdot I_{0^o}^{\prime}(Z_4))$, the binary bit will be kept unchanged after seam carving. However, for the corresponding bit of $LBP(Z_0)$, the value could be remained the same once $sign(Z_{15} - Z_0)$ is equal to $sign(Z_4 - Z_0)$ (for the detail of LBP, please refer to [42]). Therefore, compared with LBP, LDP is in general more altered to seam carving than LBP does. For this reason, it is expected that LDP could be more sensitive to the process seam carving than LBP.

In constructing LDP features, for each direction α as mentioned above, the normalized histogram of the LDPs are employed as features to reveal the statistical change introduced by seam carving. Clearly, each histogram comes up with $2^8 = 256$ bins.

To calculate the n^{th} order LDP along direction α with $n > 2$ and radius equal to 1, the $(n-1)^{th}$ order derivatives $I_\alpha^{n-1}(Z)$ along α is needed to compute firstly. For instance, to derive the 3rd order LDP of Z_0, the 2nd order derivatives $I_\alpha^{\prime\prime}(Z_0)$ along direction α is computed as

$$I_\alpha^{\prime\prime}(Z_0) = I_\alpha^{\prime}(Z_0) - I_\alpha^{\prime}(Z_i), i = 1 \dots 8. \tag{3.1}$$

Therefore, the 3rd order LDP of Z_0 can be coded similarly by Equation 2.2, and the normalized histogram of LDP could be obtained as well.

In this work, only the 2nd and the 3rd order LDP features are adopted since the discriminative information carried by the higher order LDP features could be more sensitive to the noise [44] and increase largely the feature dimensionality. Besides, multi-resolution sampling and circulate sampling is also applied. Considering the correlation of pixels could be weaken as the distance between them increases, the sampling radius is only

set to 1 and 2 for each type of LDP features, respectively. Furthermore, only $\alpha = 0^o$ and 90^o are applied because seams are deleted either horizontally or vertically from the image. Therefore, LDP features of these two directions are believed to be effective on discovering the trace of seam carving. Besides, utilizing too many types of LDP features may also bring more redundancy and increase the risk of overfitting so as to decline the performance. These have been verified by the conducted experimental works. That is, we have worked on the 4th order LDP, the radius equals to 3, and the direction α equals to 45^o or 135^o, while the feature dimensionality of the model has been dramatically increased, the detection accuracy could not be further boosted in these testing. Therefore, the proposed LDP feature set is formed with the selected types of LDP features, and the dimensionality is fixed as 2048 (i.e., 256×2×2×2).

3.1.2 Markov Features

As the image content is manipulated by seam carving, the transition probabilities of the adjacent pixels in the carved images could be different from that in the uncarved image. Therefore, it is believed that the Markov process could be utilized to reflect seam carving not only in JPEG images [30] but also in uncompressed images.

The first order Markov transition probability feature, referred to as Markov feature, has been introduced to determine JPEG steganography [31]. Denote a JPEG 2-D DCT coefficient array by F. The first order horizontal difference array $D^{\rightarrow}$, i.e., the first order derivative array along horizontal direction is:

$$D^{\rightarrow}(u, v) = F(u, v) - F(u, v + 1) \tag{3.2}$$

where u and v are the horizontal and vertical coordinates, respectively. The superscripts '$\rightarrow,\nearrow,\uparrow,\nwarrow,\leftarrow,\swarrow,\downarrow,\searrow$' indicate the orientation of the calculation. Then, a threshold T_1 is selected to limit the value of each element of difference arrays within the range of $[-T_1, T_1]$ in order to reduce the computational complexity without losing much useful information. Therefore, the 1st order Markov feature along horizontal direction $M^{\rightarrow}_{a,b}$ can be denoted as:

$$M^{\rightarrow}_{a,b} = p^{\rightarrow}\{D^{\rightarrow}(u,v+1) = a | D^{\rightarrow}(u,v) = b\} = \frac{\sum_{u,v}\delta(D^{\rightarrow}(u,v) = b, D^{\rightarrow}(u,v+1) = a)}{\sum_{u,v}\delta(D^{\rightarrow}(u,v) = b)},$$

$$\delta(D_1 = a, D_2 = b) = \begin{cases} 1, & if D_1 = a, D_2 = b \\ 0, & otherwise \end{cases} \quad (3.3)$$

where $a, b \in \{-T_1, \dots, 0, \dots T_1\}$. The dimensionality of each Markov feature is $(2T_1 + 1)^2$. Similarly, the 1st order Markov feature along '$\nearrow$', '$\downarrow$' and '$\searrow$' directions can be calculated. In this work, all four directions' Markov features are adopted which resulting in a $4 \times (2T_1 + 1)^2$ dimensional feature vector.

3.1.3 SPAM Features

In addition to the 1st order In addition to the 1st order Markov features discussed above, the seam carving can also be captured by the higher order Markov process. However, the dimensionality of Markov feature increases exponentially with order. Due to the computation complexity, 2nd order SPAM [49] features are applied instead of 2nd order Markov features because the SPAM features are linear combinations of the 2nd order

Markov features along 8 directions. Therefore, the discriminative information carried by Markov features could also be reflected by SPAM features with the same order.

To calculate the 2nd order SPAM feature of a given image I, the difference arrays and the transition probability matrixes of 8 directions are computed firstly. Then, the 2nd order horizontal Markov feature $M^{\rightarrow}_{a,b,c}$ is calculated as follows

$$M^{\rightarrow}_{a,b,c} = p^{\rightarrow}\{D^{\rightarrow}(u,v+2) = a | D^{\rightarrow}(u,v+1) = b, D^{\rightarrow}(u,v) = c\} \quad (3.4)$$

where $a, b, c \in \{-T_2, \dots, 0, \dots T_2\}$. The 2nd order Markov feature along other directions: '↗ ,↑,↖,←,↙,↓,↘' can be derived likewise. Finally, by averaging 2nd order Markov feature along '→,←,↑,↓' and '↗,↙,↖,↘' separately, the 2nd order SPAM feature is formed of those two averaged Markov feature sets, and the dimensionality is $2 \times (2T_2 + 1)^3$. In the experiments, the thresholds T_1 and T_2 are set following [31] and [49] where $T_1 = 4$ which leading to a 324-D Markov feature vector, and $T_2 = 3$ for the 2nd order SPAM features, which resulting in a 686-D feature vector. Both types of features are intuitively extracted from spatial domain because seam carving is also conducted in spatial domain and the images are uncompressed.

3.1.4 SVM-Recursive Feature Elimination

As previously introduced, the proposed feature model is consisting of three types of features, resulting in a relatively high dimensional feature set. Therefore, in order to reduce the feature redundancy, hence reduce feature dimensionality and computational complexity, an effective feature selection method is applied to the proposed feature model. In this work,

the linear support vector machine based recursive feature elimination (SVM-RFE) [50] is employed for this purpose. The main idea of SVM-RFE algorithm is to eliminate one feature at a time which has the minimum ranking criterion [50], and put the eliminated feature on the top of the predefined ranking list. By recursively doing so, a feature ranking list is generated. Then, a low dimensional subset, composed by only taking certain number of top ranked features in the list, is selected for the classification instead of the original feature set of high dimensionality. For linear SVM classifier, the ranking criterion C is given by

$$C = (w)^2, \quad w = \sum_k \alpha_k y_k x_k \tag{3.5}$$

where α_k is the Lagrange multiplier, y_k is the class label of corresponding sample x_k, and the weight vector w is a linear combination of training patterns. The procedure of the SVM-RFE is as follows.

Given:

Training samples $X = [x_1, x_2, \dots, x_n]$;

Each sample x is a l-dimensional vector with feature S

$S = [s_1, s_2, \dots, s_l]$;

Class labels $Y = [y_1, y_2, \dots, y_n]$;

Ranking list $R = [\,]$;

Step 1: Train SVM $\alpha = SVM(X, Y)$;

Step 2: Calculate C by (12) and find s_t with smallest C

$$s_t = arg\,min(C);$$

Step 3: Remove s_t *from S*

$$S = [s_1 : s_t, s_{t+1} : s_l];\ R = [s_t, R];$$

Step 4: If $S = [\ ]$, *break, return R;*

Else, go to Step 1.

It is known that the feature with a higher ranking does not necessarily mean it has better performance than a lower ranked feature. However, a subset gathering the top ranked features is optimal [50]. Hence, instead of applying the original high dimensional feature set for classification, a subset only consists of high ranked features could lead to a better result. In the experiments, several feature subsets have been investigated and the performance has demonstrated the effectiveness of the feature selection mentioned above.

3.2 Experimental Results

In this work, the seam carved image database has been established in the previous work, i.e., twelve different seam carving image sets, is utilized to evaluate the performance of the proposed method. Lib-SVM library [46] has been also utilized in the experiments and linear kernel with default parameters has been applied. Furthermore, each reported result is the average detection accuracy over 10 iterations of 6-fold cross validation.

3.2.1 Performance of 3058-D Feature Model without SVM-RFE

Firstly, we investigate the performance of each of these three kinds of feature components, i.e., LDP features, Markov features and SPAM features, individually. Observed from Figure 3.2, the 2048-D LDP features achieve the best performance among these three

feature components. Furthermore, the proposed 3058-D feature model outperforms each of these three kinds of feature components in detecting most of seam carving cases. However, the performance of 3058-D model is close to or even lower than that achieved by the LDP features on high carving rate cases. On the one hand, it is clear that the LDP features contribute most among these three feature components, and the 3058-D model does perform better than each individual component does. On the other hand, the redundancy of proposed 3058-D model could lead to overfitting in classification and hence influence the overall performance especially on detecting high carving rate cases.

To compare the performance of the proposed 3058-D feature model with the state-of-the-art, the methods proposed in [40, 41] have been implemented and tested on the same dataset. As observed from Figure 3.3, the detection accuracy increases with the carving rate for all methods because more image content are removed for high carving rate cases and more artifacts are thus introduced. On the contrary, due to less artifacts are introduced in a seam carved image with low carving rate, the traces are much more difficult to detect. Obviously, although the performance of the method reported in [41] is slightly better on detecting large carving rate cases, the proposed 3058-D model outperforms other three methods on cases with a carving rate lower than 30%, especially for ‘5%H’ and ‘10%H’ on which the 3058-D model outperforms other methods by more than 10%. Next, the detection accuracies averaged over horizontal and vertical directions for these four schemes are compared in Table 3.1. It observed that on detecting 5%, 10% and 20% carving rate cases the best performance of [40, 41] is 66%, 75% and 87%, respectively; while the

Table 3.1 Average Detection Accuracy of Proposed 3058-D Model versus the State-of-the-Art.

	5%	10%	20%	30%	40%	50%
Ryu et al. (2014)	65.89%	75.15%	85.79%	92.11%	95.26%	97.25%
Yin et al. (2015)	58.72%	70.22%	87.37%	95.63%	**98.58%**	**99.51%**
Proposed 3058-D	**76.67%**	**85.94%**	**93.29%**	**96.59%**	97.97%	98.92%

proposed 3058-D feature model achieves 76%, 85% and 93%, respectively. This indicates that the proposed 3058-D feature model is powerful in acquiring minute traces of seam carving, especially at the low rate seam carving. The reason the other two compared methods can achieve relatively good performance on detecting high carving rate cases is because both of them utilize energy based features, such as average energy of the columns and average energy of the rows. Since pixels with low energy would have more chances to be deleted by seam carving process, the difference of the average pixel energy between un-seam carved images and seam carved images could be significant when carving rate is sufficiently high. Therefore, energy based features could have good performance on detecting high carving rate cases.

Another observation is that the proposed approach always achieves better performance in detecting ‘vertical carving’ (width shrinking) than that on detecting ‘horizontal carving’ (height shrinking) at a same carving rate. The reason behind is the UCID database consisting of 1338 images where 453 images have a size of 512 × 384 (height × width) and the rest 885 images are 384 × 512. Intuitively, for an image with a larger width than height, e.g., an image with a size of 384 × 512, more seams need to be carved via ‘vertical carving’ than via ‘horizontal carving’ when the carving rate is fixed.

Therefore, ‘vertical carving’ could have more chance to introduce a significant change to the relation of the remaining pixels in this kind of image than ‘horizontal carving’. On the contrary, ‘horizontal carving’ could be more detectable than ‘vertical carving’ with a fixed carving rate when the original image has a larger height than width, e.g., the image with a size of 512 × 384. Since UCID database contains more images with a larger width, the performance of proposed method on detecting vertical carving is in general better than detecting horizontal carving.

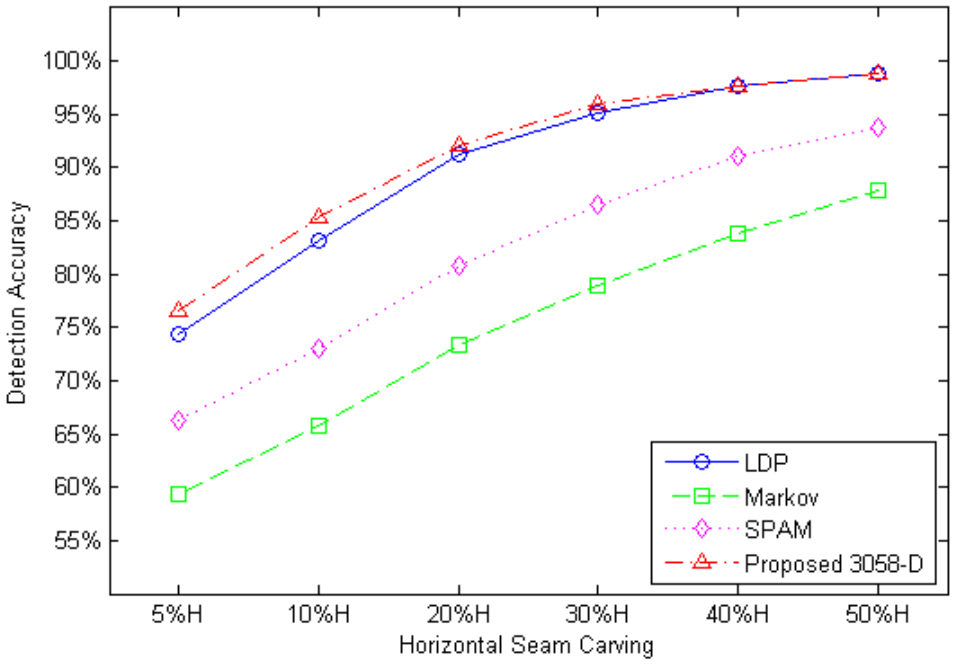

(a)

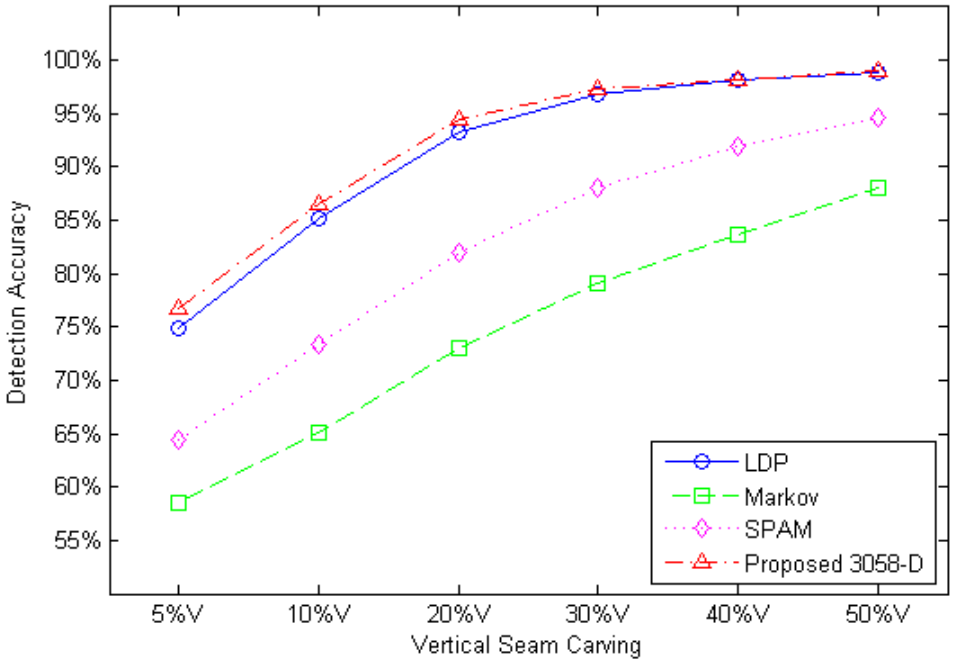

(b)

Figure 3.2 Detection accuracy of each kind of feature component versus proposed 3058-D model on detecting 12 different seam carving scenarios.

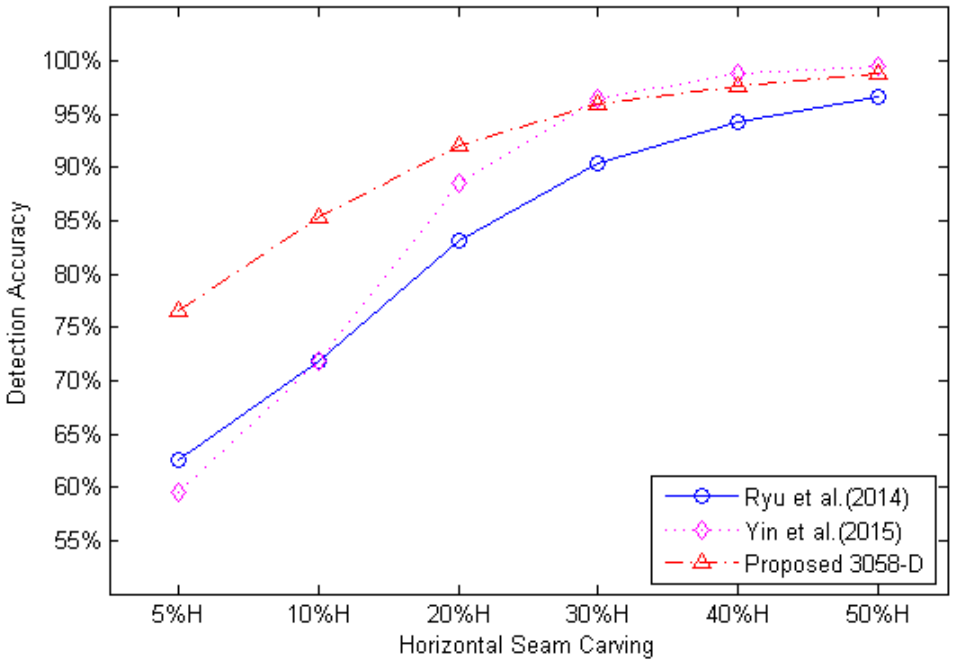

(a)

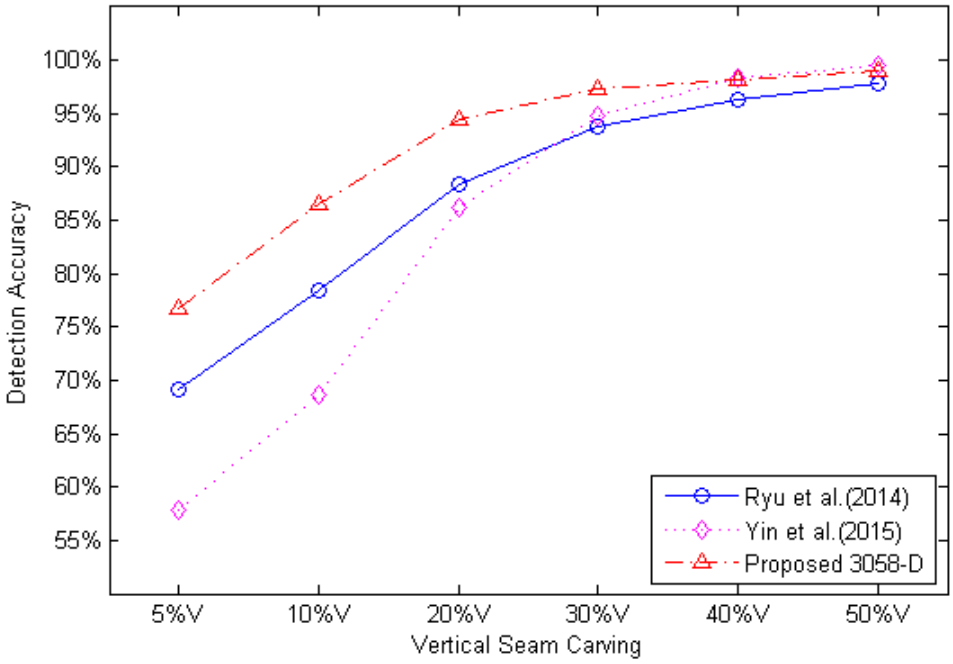

(b)

Figure 3.3 Detection accuracy of proposed 3058-D model versus the state-of-the-art on detecting 12 different seam carving scenarios.

3.2.2 Performance of 3058-D Model with SVM-RFE

To improve the performance achieved by the 3058-D model, the SVM-RFE is proposed to apply. For detecting each type of seam carving, an extra training process is conducted for SVM-RFE. Following the top to bottom order of the ranking list output by SVM-RFE, a feature subset is formed with features selected from the original 3058-D model. Then, the feature subset is utilized to replace the original 3058-D feature model in the classification. In the experiments, four feature subsets including 100-D, 200-D, 500-D and 1000-D have been investigated, respectively, where '100-D' stands for feature subset formed with the top 100 features on the ranking list, so as others. Observed from Figure 3.4, most of the investigated feature subsets outperform the original 3058-D model and the state-of-the-art on all seam carving cases except 100-D is slightly worse than proposed 3058-D model on cases with a carving rate lower than 30%. Notably, for the tough cases, i.e., cases with a carving rate less or equal to 10%, the performance monotonically increasing when more feature are selected. However, for cases with a carving rate larger than 20%, the fact is that more features do not bring more satisfactory performance, e.g., only 200 selected features can provide a fairly promising detection accuracy and outperform the state-of-the-art when carving rate is higher than 20%. After investigating the training results, we could conclude that a more complex model could be more likely lead to overfitting on detecting cases with a high carving rate, while it could have better performance on detecting low carving rate cases. As shown in Table 3.2, by applying the SVM-RFE, the average detection accuracies achieved by proposed approach on the same carving rate cases could be boosted from 76%, 85% and 93% on detecting 5%, 10% and 20% carving rate cases to 81%, 90% and 96%, respectively. As illustrated in Figures 3.5, 3.6, and 3.7, each tested feature subset, i.e., 200-

D, 500-D, and 1000-D, outperforms the proposed 3058-D model on cases with a carving rate lower than 30%, while the 3058-D model has a significantly better performance than the other two methods on these cases. As the carving rate is getting higher, the gap between all tested methods is getting smaller. As a conclusion, with the help of SVM-RFE, the performance of 3058-D feature model can be improved effectively, and 500-D gives the best overall performance according the experiments.

Table 3.2 Average Detection Accuracy of Feature Subsets Selected by SVM-RFE versus Original 3058-D Model.

	5%	10%	20%	30%	40%	50%
3058-D	76.67%	85.94%	93.29%	96.59%	97.97%	98.92%
200-D	78.37%	88.07%	94.67%	97.79%	99.13%	**99.65%**
500-D	81.13%	90.26%	**96.04%**	**98.38%**	**99.26%**	99.62%
1000-D	**81.49%**	**90.72%**	96.01%	98.33%	99.17%	99.64%

3.2.3 Analysis of Ranking Lists

In order to demonstrate the necessity of all three feature components, the ranking lists trained by SVM-RFE are analyzed. In Figure 3.8, the distribution of LDP, Markov and SPAM features in 200-D and 500-D feature subsets are shown. It is clearly that, even though the original feature set has been reduced significantly by SVM-RFE, none of these three feature components is excluded from the finalized feature subsets. They all contribute to the detection accuracies, and they are complimentary to each other as expected.

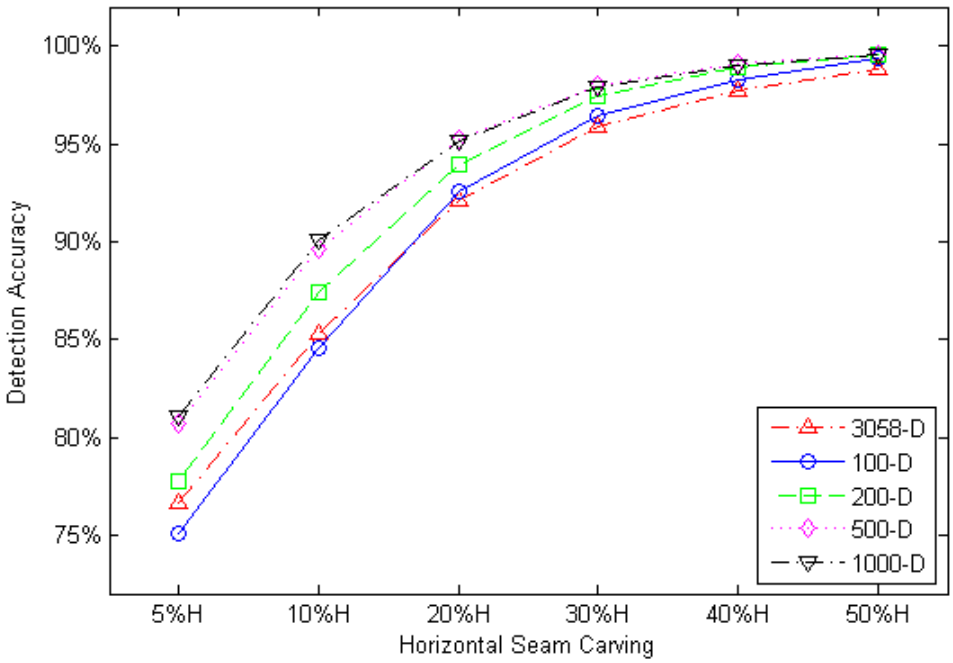

(a)

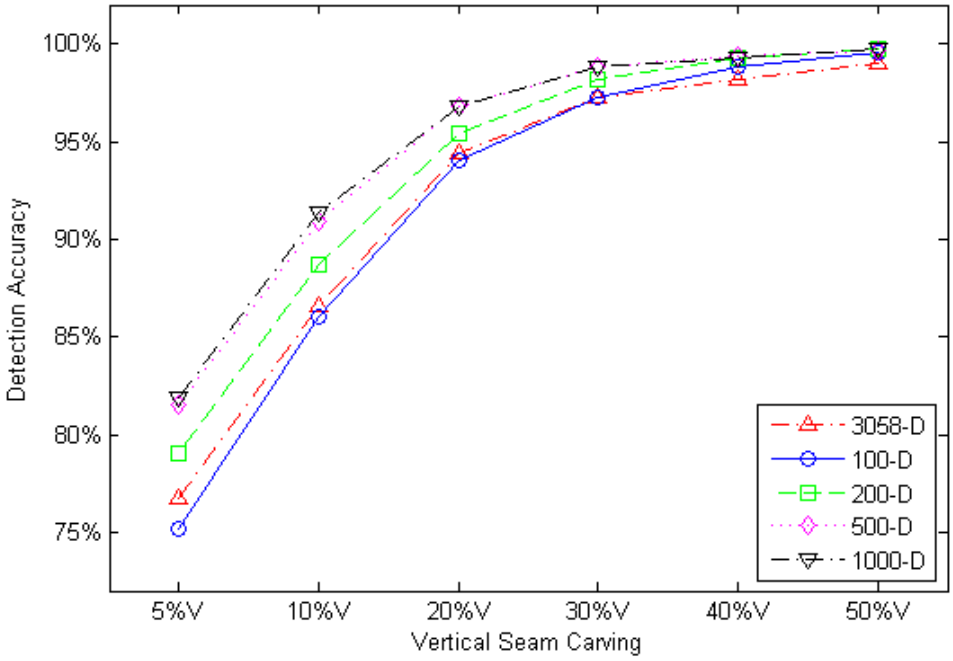

(b)

Figure 3.4 Detection accuracy of feature subsets selected by SVM-RFE versus original 3058-D model on detecting 12 different seam carving scenarios.

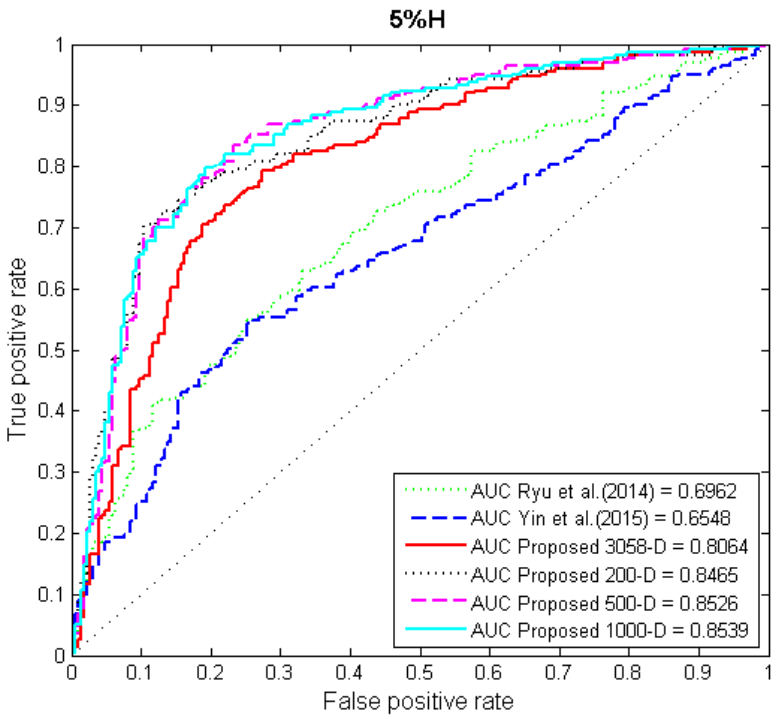

(a)

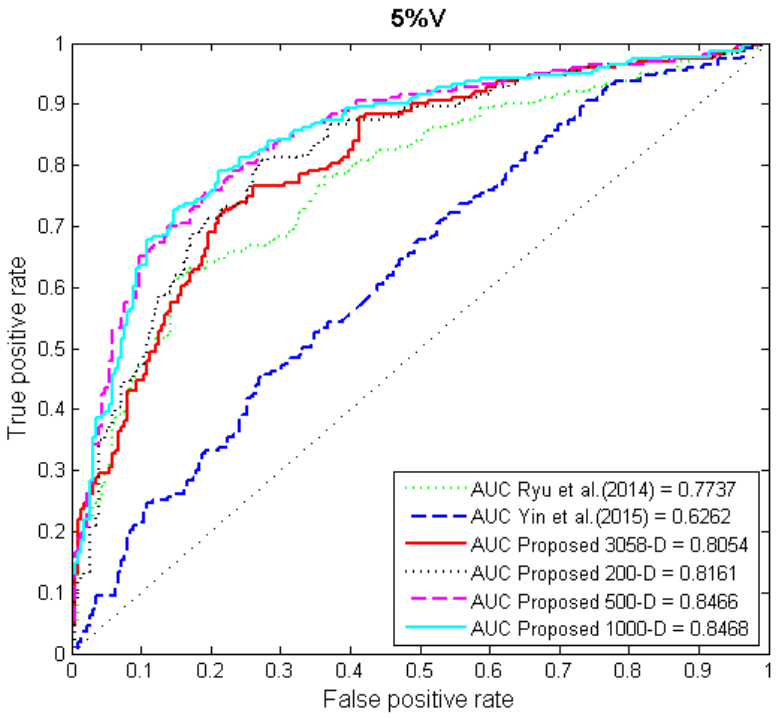

(b)

Figure 3.5 ROCs of all compared methods on detecting seam carving at carving rate as 5%.

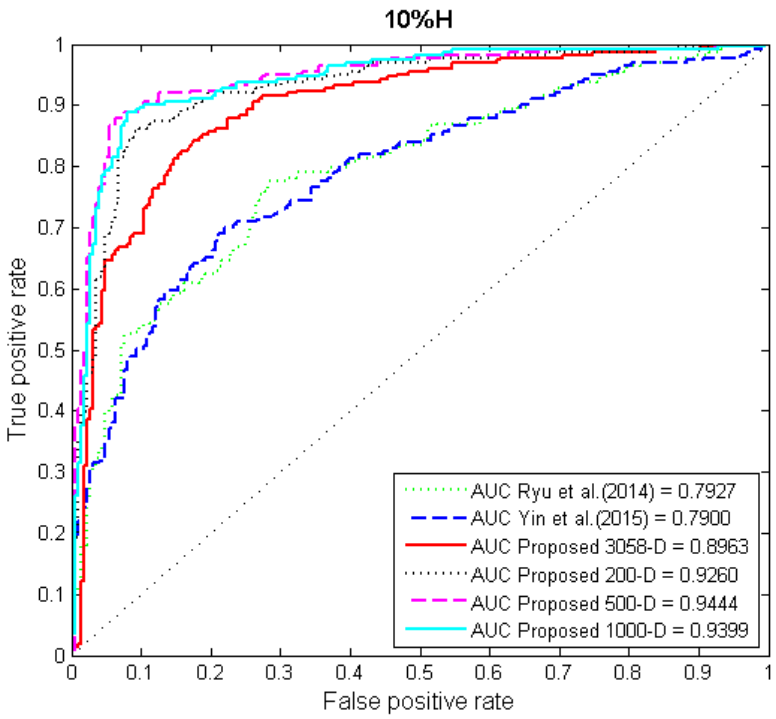

(a)

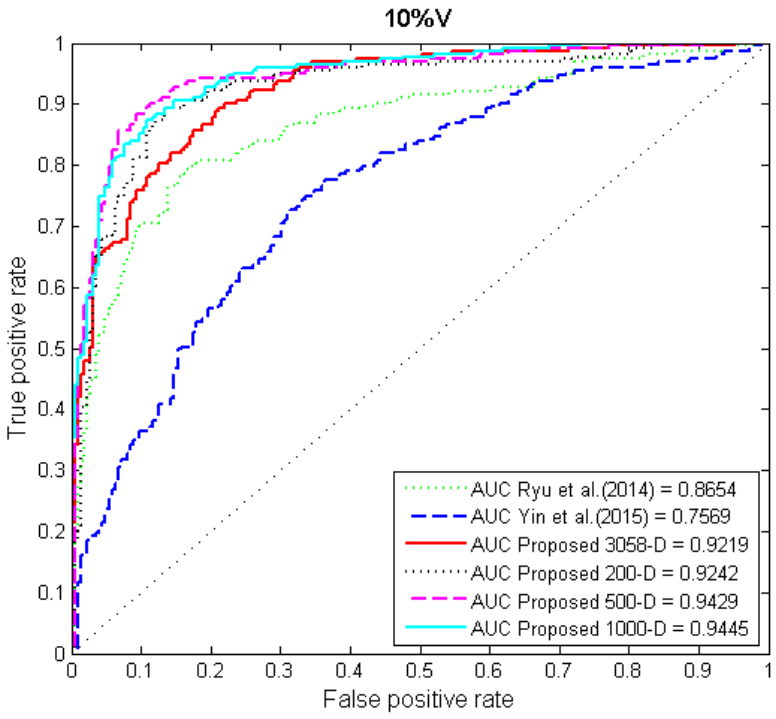

(b)

Figure 3.6 ROCs of all compared methods on detecting seam carving at carving rate as 10%.

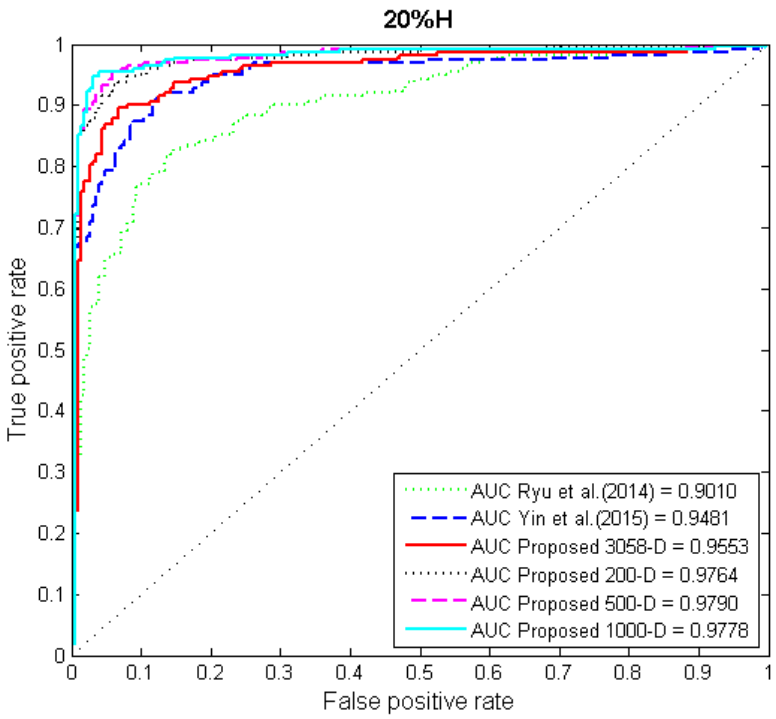

(a)

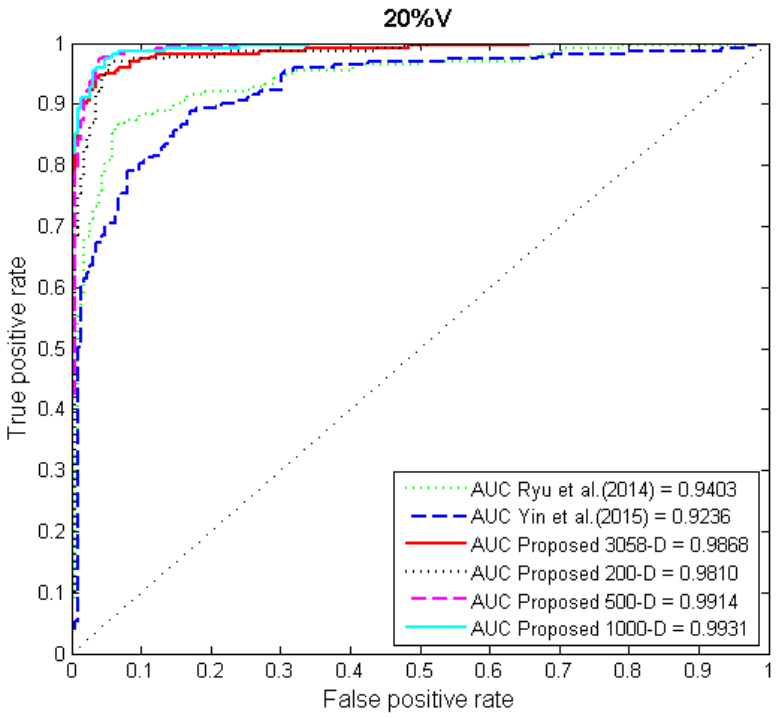

(b)

Figure 3.7 ROCs of all compared methods on detecting seam carving at carving rate as 20%.

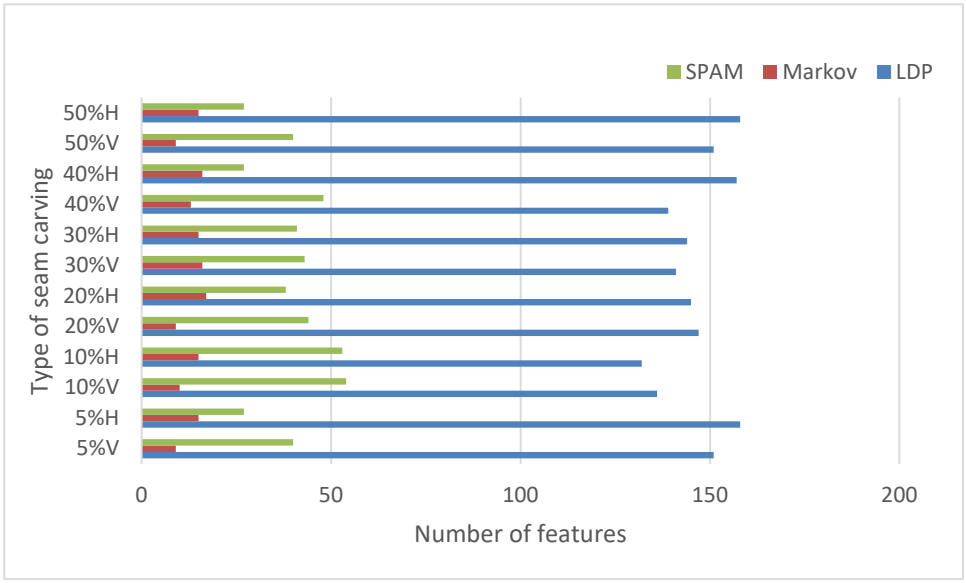

(a)

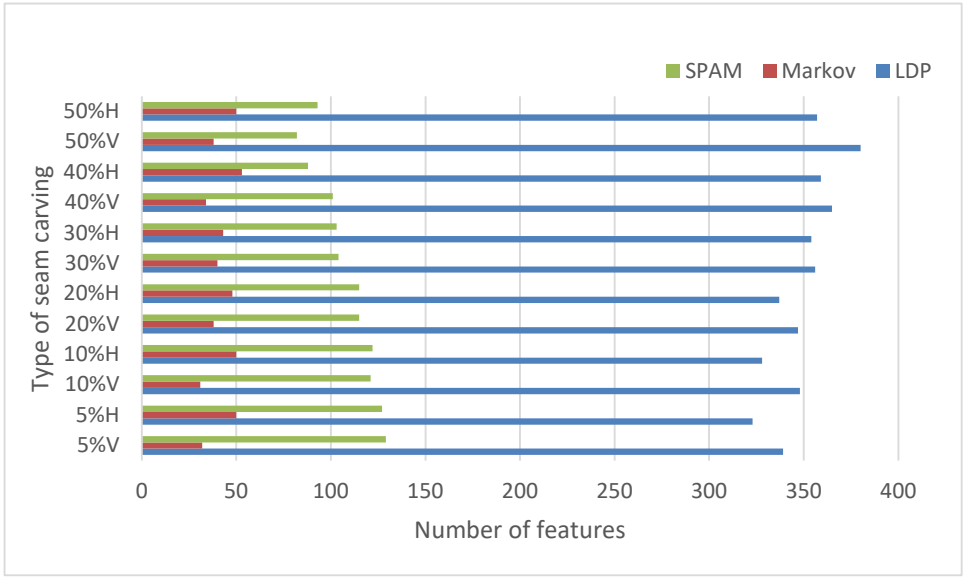

(b)

Figure 3.8 Distribution of LDP, Markov and SPAM feature in 200-D (a) and 500-D (b) feature set for detecting each type of seam carving set.

3.2.4 Performance of Proposed Method on Mix Set

To further investigate the robustness and generality of the proposed method, another test on a mixed image set was conducted. In Table 3.3, each result is also the average detection accuracy over 10 iterations of 6-fold cross validation. For each iteration, 1/12 samples were randomly selected from each of the 12 previously established seam carving image sets to form the mixed seam carving image set while each sample in the mix set was generated from different original image. From Table 3.3, it is observed that the proposed original 3058-D model achieves 91% detection accuracy while the best result of the state-of-the-art is 86%. By applying SVM-RFE, the detection accuracy of proposed method can be boosted to 92% on the Mix set, and the feature dimensionality of proposed 3058-D model can be dramatically reduced. Obviously, the proposed method is more robust and general than the state-of-the-art even without applying feature selection.

Table 3.3 Detection Accuracy of all Compared Methods on Mix Set.

	Ryu et al.	Yin et al.	3058-D	100-D	200-D	300-D	400-D	500-D	1000-D
Mixed	78.96%	86.31%	91.25%	90.28%	91.51%	92.22%	92.58%	**92.56%**	92.59%

3.2.5 Performance of 3058-D Model on Detecting Seam Carving in JPEG Images

As known, JPEG images, are widely used in daily life nowadays. For that reason, the proposed 3058-D feature model is also tested against seam carving in JPEG images.

The JPEG database is established based on UCID dataset with the same manner as presented in [41]. Each image of UCID dataset is JPEG compressed with quality factor (QF) equal to 70 in MATLAB, thus to form the un-seam carved JPEG image set. Then,

each image from the un-seam carved set is decompressed and modified by seam carving with various carving rates, i.e., 5%, 10%, 20%, 30%, 40% and 50%, and two carving directions, i.e., horizontal or vertical. After that, each seam carved image is recompressed with the same QF as that used in the first compression. Consequently, 12 seam carved JPEG image sets are built.

From Figure 3.9, it is observed that the proposed 3058-D feature model can also achieve remarkable performance on detecting seam carving in JPEG images. Concretely, the 3058-D model can detect low carving rate cases better than the other two methods. Similarly to the test results on uncompressed image sets, the energy based approaches, i.e., [40, 41], have better performance on detecting high carving rate cases than the 3058-D model.

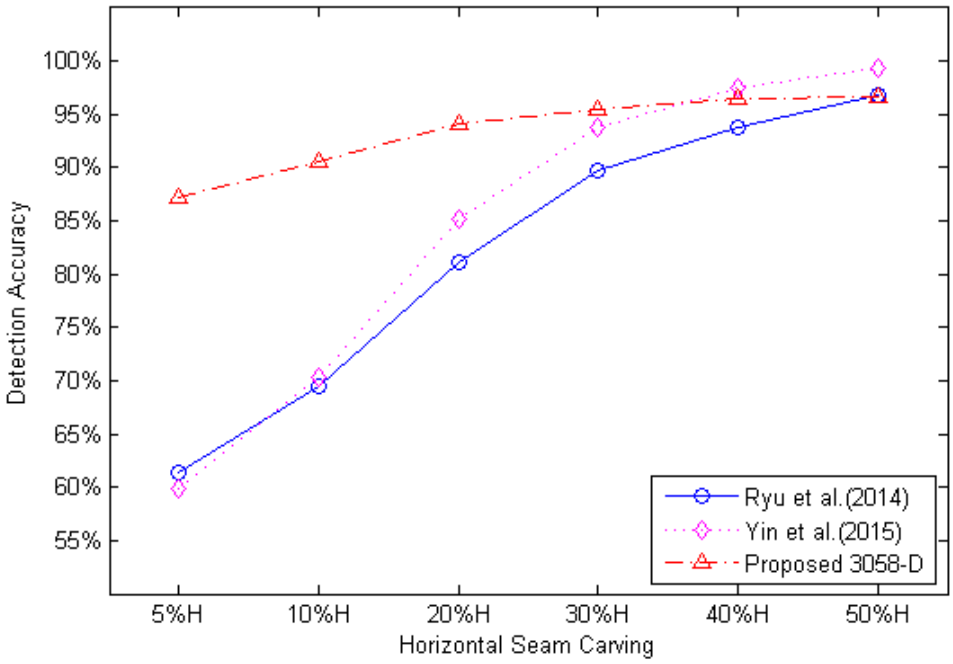

(a)

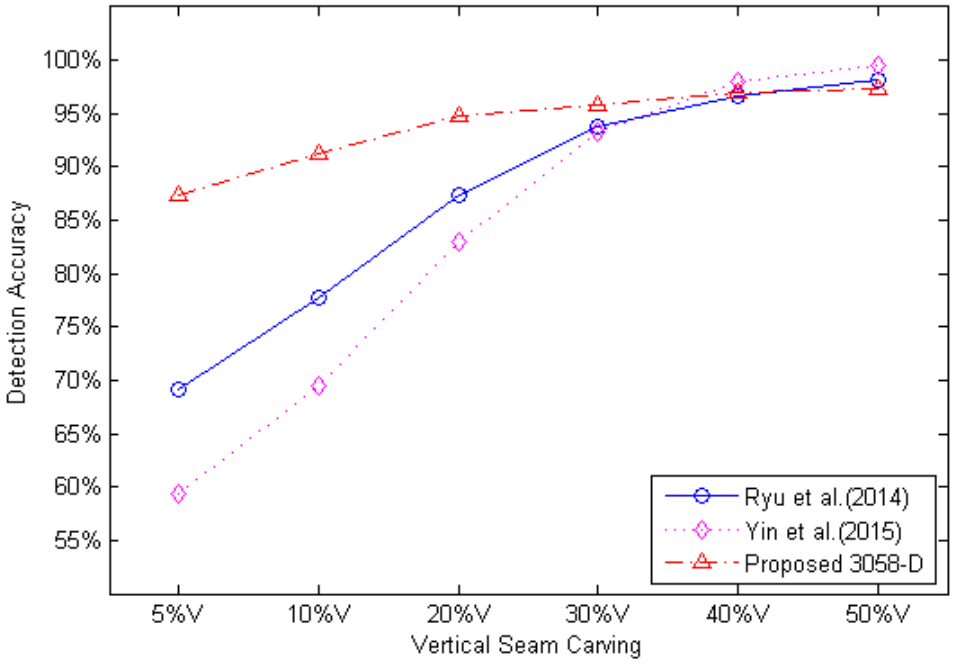

(b)

Figure 3.9 Detection accuracy of proposed 3058-D model versus other methods on detecting seam carving in JPEG images with QF=70.

3.2.6 Performance of 3058-D Model on Detecting Seam Carving in Rotated Images and Rescaled Images

Additionally, we conducted a series of experiments to investigate if our proposed 3058-D model is robust to geometric transforms, i.e., image rotation and scaling. The image sets are generated based on our pre-established uncompressed seam carving sets. For the rotated-image sets, each of the un-seam carved images and seam carved images are rotated clockwise with an angle of 30^o or 60^o, respectively. For the rescaled image sets, each image is rescaled with a scaling factor of 0.9 and 1.1, respectively. All the process is conducted in MATLAB and bilinear interpolation is applied. Observed from Table 3.4 and 3.5, although on low carving rate cases the detection accuracies are degraded, the overall performance of the proposed 3058-D model is still promising.

Table 3.4 Detection Accuracy of Proposed 3058-D Model on Detecting Seam Carving in Rotated Images.

Angle	5%H	10%H	20%H	30%H	40%H	50%H
30^o	72.53%	83.15%	95.10%	98.37%	99.26%	99.67%
60^o	72.59%	84.19%	95.63%	98.39%	99.19%	99.66%

Angle	5%V	10%V	20%V	30%V	40%V	50%V
30^o	69.96%	84.01%	95.44%	98.47%	99.26%	99.62%
60^o	71.39%	84.26%	95.65%	98.20%	99.21%	99.67%

Table 3.5 Detection Accuracy of Proposed 3058-D Model on Detecting Seam Carving in Rescaled Images.

Scale	5%H	10%H	20%H	30%H	40%H	50%H
0.9	67.15%	76.51%	85.71%	91.93%	94.90%	96.66%
1.1	71.47%	80.30%	89.68%	94.05%	96.76%	97.82%

Scale	5%V	10%V	20%V	30%V	40%V	50%V
0.9	66.77%	74.84%	86.18%	92.90%	95.96%	97.77%
1.1	74.73%	82.09%	91.86%	95.28%	96.85%	98.21%

3.3 Conclusion

In this chapter, an advanced statistical feature model consisting of LDP features, Markov features and SPAM features is proposed to detect seam carving in uncompressed grayscale images. The experimental results have indicated the proposed 3058-D feature model outperforms the state-of-the-art on detecting the low carving rate images. By applying SVM-RFE, the proposed approach can be improved and the detection accuracy on low carving rate cases such as 5%, 10% and 20% is boosted to 81%, 90% and 96%, respectively, while the prior state-of-the-art has 66%, 75% and 87%, respectively, accuracy on the same cases. The experimental results also illustrate that the proposed 3058-D feature model are capable to detect seam carving process in JPEG images, and robust to geometrical transforms, i.e., image rotation and scaling.

CHAPTER 4

A HYBRID FEATURE MODEL FOR SEAM CARVING DETECTION

So far, two different feature models have been presented in this dissertation to reveal the process of seam carving applied to digital images. By seizing the statistical variation of energy distribution caused by seam carving, the first proposed method, i.e., the 96-D feature model, is able to differentiate seam carved images from non-seam carved ones. From a different perspective, the 3058-D model is later presented to catch the changes of the relationship between neighboring pixels so as to decide whether an image has gone through seam carving or not. Both methods have been achieved remarkable performance in the experimental works. In this chapter, an advanced feature model is designed based on the ideas behind aforementioned two feature models so as to further improve the detection accuracy against seam carving at low carving rate, e.g., such as 5% and 10%. To construct the proposed model, the features included in the 3058-D model are all adopted, and 180 features are inspired by the 96-D model. By introducing twelve new features to capture the energy changes of the optimal quarter and three-quarter seams, and applying the energy features extracted from spatial domain, the dimensionality of the 96-D model has been increased to 180. According to the experimental results, the proposed hybrid feature model has achieved remarkable performance on detecting low carving rate cases. The detail of the proposed feature model is introduced in Section 4.1. In Section 4.2, the experimental results are reported, then the conclusion is made in Section 4.3.

4.1 Proposed Feature Model

As proved in Chapter 3, it is effective on determining whether a digital image has been seam carved or not by employing powerful features which can reflect the variation of relationship between neighboring pixels, such as the proposed 3058-D feature model. Also, the 96-D feature model has shown the efficiency on tracking the trace of seam carving in an image through investigating the changes of energy distribution. Although both methods have been achieved better performance comparing with the state-of-the-art in the conducted experimental works, the performance on detecting seam carved images with low carving rate, such as 5% and 10%, is still need to be further improved because these cases are considered more important, and more general in real life. Therefore, an advanced feature model, i.e., 3238-D feature model, is presented in this chapter for seam carving detection.

The proposed 3058-D feature model consists of two groups of features: one group of features is utilized for monitoring the statistical changes of relationship between local pixels, while another group is utilized for measuring the changes of energy distribution of an image. To form the first group of features, the previously proposed 3058-D model is adopted due to its remarkable performance as reported in Chapter 3. Noted, since it has been also indicated in the experiment works that the performance of the 3058-D model could not be further improved by adding more similar features, such as LDP features with higher orders or larger radius, the 3058-D model is kept without any changes accordingly (refer to Chapter 3).

As presented in Chapter 2, in order to obtain the 96-D feature vector, the input image is firstly pre-processed by four different LDP operators to produce four LDP images.

Then, 24 features are extracted from each LDP image, thus total 96 features are acquired. In the proposed feature model, the way how the 96 features are extracted is also followed and the 96 features are all included. Besides, in addition to the set of 24 features, another 12 newly designed features are proposed to be extracted from each LDP image as well. As illustrated in Table 4.1, six features are proposed to measure the energy of the optimal quarter seams in the image, while the other six features are measuring the energy of the optimal three-quarter seams. Therefore, a 36-D feature vector is acquired for each LDP images. Furthermore, a set of 36 features is extracted from the original input image. Consequently, five sets of 36 features, as shown in Figure 4.1, can be obtained for each input image to capture the changes caused by seam carving from the view of energy distribution, and the obtained total 180 features form the second group of features in the proposed feature model.

By combining the above presented two groups of features, i.e., 3058-D and 180-D, the proposed feature model is formed with a dimensionality as 3238 in total, and whole framework is illustrated in Figure 4.2.

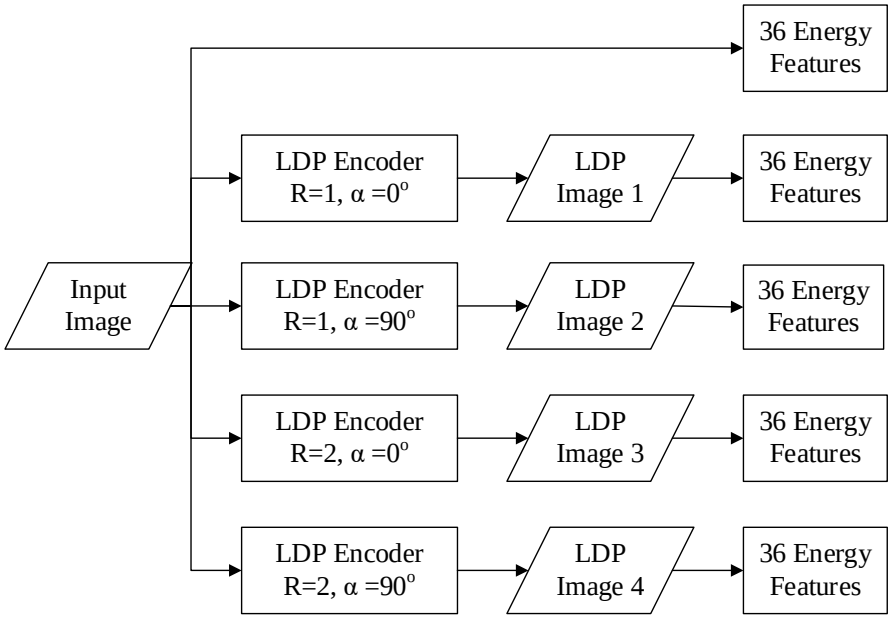

Figure 4.1 Feature formation procedure of proposed 180 energy features.

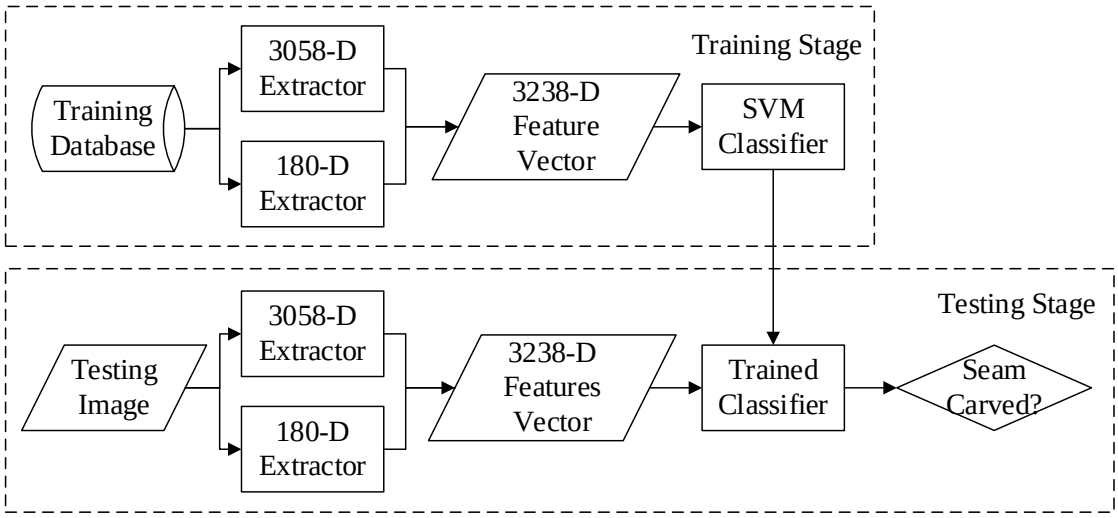

Figure 4.2 Framework of proposed 3238-D feature model.

Table 4.1. Description of 12 Energy Features

Feature	Description
1. Quarter Horizontal Seam$_{max}$	$max_{i=1}^{m} M(i, \frac{n}{4})$
2. Quarter Horizontal Seam$_{min}$	$min_{i=1}^{m} M(i, \frac{n}{4})$
3. Quarter Horizontal Seam$_{mean}$	$\frac{1}{m}\sum_{i=1}^{m} M(i, \frac{n}{4})$
4. Quarter Vertical Seam$_{max}$	$max_{i=1}^{n} M(\frac{m}{4}, i)$
5. Quarter Vertical Seam$_{min}$	$min_{i=1}^{n} M(\frac{m}{4}, i)$
6. Quarter Vertical Seam$_{mean}$	$\frac{1}{n}\sum_{i=1}^{n} M(\frac{m}{4}, i)$
7. Three-Quarter Horizontal Seam$_{max}$	$max_{i=1}^{m} M(i, \frac{3n}{4})$
8. Three-Quarter Horizontal Seam$_{min}$	$min_{i=1}^{m} M(i, \frac{3n}{4})$
9. Three-Quarter Horizontal Seam$_{mean}$	$\frac{1}{m}\sum_{i=1}^{m} M(i, \frac{3n}{4})$
10. Three-Quarter Vertical Seam$_{max}$	$max_{i=1}^{n} M(\frac{3m}{4}, i)$
11. Three-Quarter Vertical Seam$_{min}$	$min_{i=1}^{n} M(\frac{3m}{4}, i)$
12. Three-Quarter Vertical Seam$_{mean}$	$\frac{1}{n}\sum_{i=1}^{n} M(\frac{3m}{4}, i)$

4.2 Experimental Results

To evaluate the performance of proposed 3238-D feature model, the same database utilized in Chapters 2 and 3, i.e., 12 different seam carving scenarios and each has 1338 uncompressed grayscale images, is employed. Furthermore, since it has been indicated in the conducted experiments of previous chapters that both 96-D and 3058-D models outperform the state-of-the-art, the proposed 3238-D model is only compared with the two models aforementioned, and the enhanced model of 3058-D, i.e., 500-D feature model which has been presented in Chapter 3. The reason 500-D model is picked for comparison is that it has been achieved the best results as reported in Chapter 3. Lib-SVM with linear kernel is adopted as the classifier, while all reported accuracies are based on the average results of 10 times' 6-fold validation strategy.

As illustrated in Figure 4.3, it is observed that the proposed 3238-D model is much more effective versus 96-D model and 3058-D model on detecting seam carving images with a carving rate lower than 30%. In particular, as reported in Table 4.2, 96-D and 3058-D can only achieve 73.03% and 76.67% average detection accuracies on detecting seam carving with a carving rate as 5%, respectively, while the performance has been boosted to 85.75% by the proposed 3238-D model. Similarly, the average detection accuracy achieved by 3238-D is 6% higher than the best of 96-D and 3058-D on detecting cases with a carving rate equal to 10%. Moreover, 3238-D outperforms 500-D on detecting all designed seam carving scenarios, and the average detection accuracies achieved by 3238-D on detecting 5% and 10% carving rate cases are 4% higher that achieved by 500-D. The ROC curves shown in Figures 4.4 and 4.5 also indicated that the proposed 3238-D model is more

reliable and effective on revealing seam carving at low carving rate versus the other three models as expected.

It is also noted, although the 3238-D model has been dominated on discriminating seam carved images at low carving rate from un-carved images, the 96-D model have been achieved almost equal performance, or even better, as that achieved by 3238-D on detecting high carving rate cases, particularly cases at a carving rate as 40% and 50%. To reveal the reason behind such observation, the performance has been achieved by the 96-D model, the 3058-D model, and the 3238-D model during the training is investigated and reported in Table 4.3. As shown in Table 4.3, the 3238-D model has achieved the best training performance, and the training accuracy reaches 100% when carving rate is higher than 20%. Obviously, because the 3238-D model is more advanced and more complex than the 98-D model, the overfitting is more significant when 3238-D is applied. It should be also aware that even though the 3238-D over modeled the training data, it has outperformed other existing methods on most of designed seam carving scenarios, especially when the carving rate is as low as 5% or 10% which are considered more general in real life and more difficult to be detected.

Table 4.2 Average Detection Accuracy of Proposed 3238-D Feature Model versus the State-of-the-Art.

	5%	10%	20%	30%	40%	50%
96-D	73.03%	88.88%	97.78%	99.44%	**99.91%**	**99.96%**
3058-D	76.67%	85.94%	93.29%	96.59%	97.97%	98.92%
500-D	81.13%	90.26%	96.04%	98.38%	99.26%	99.62%
3238-D	**85.75%**	**94.87%**	**98.91%**	**99.65%**	99.89%	99.94%

Table 4.3 Average Training Accuracy of Proposed 3238-D Feature Model versus the State-of-the-Art.

	5%	10%	20%	30%	40%	50%
96-D	73.76%	89.69%	98.14%	99.68%	99.94%	99.98%
3058-D	89.47%	96.01%	99.09%	99.73%	99.99%	**100.00%**
3238-D	**96.46%**	**99.43%**	**99.98%**	**100.00%**	**100.00%**	**100.00%**

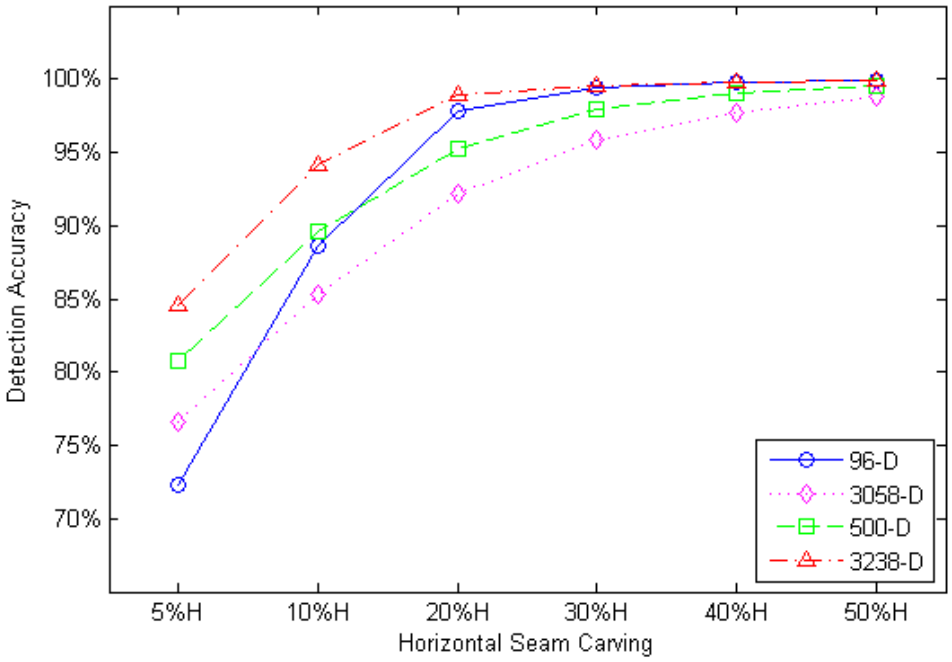

(a)

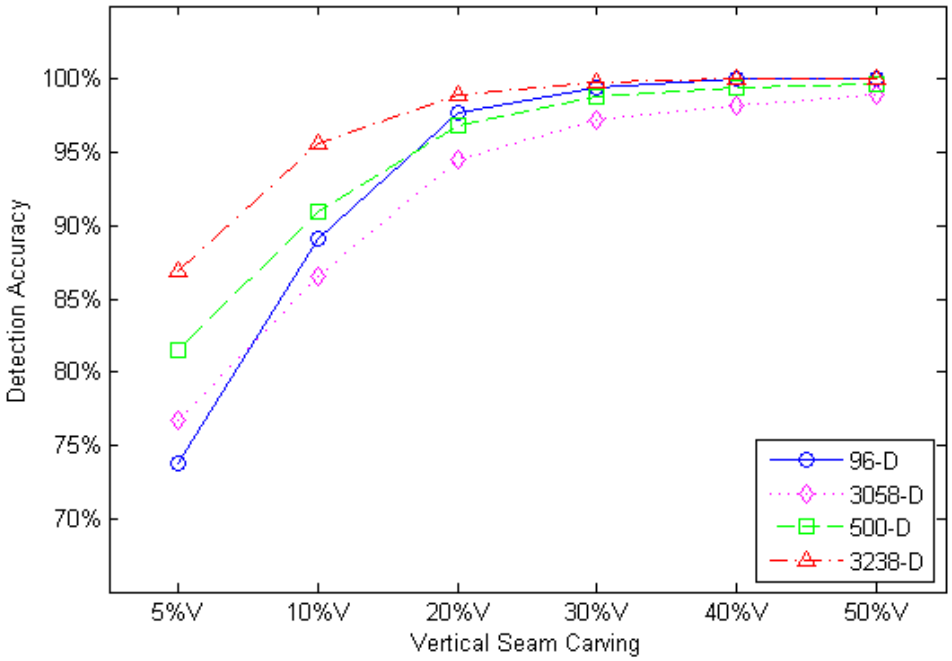

(b)

Figure 4.3 Performance of proposed 3238-D model versus the state-of-the-art on detecting 12 different seam carving scenarios.

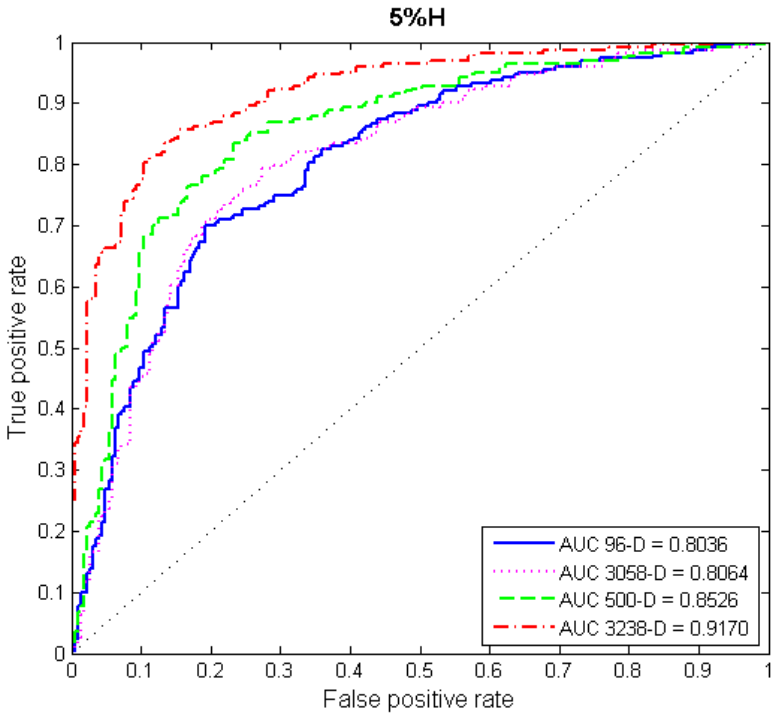

(a)

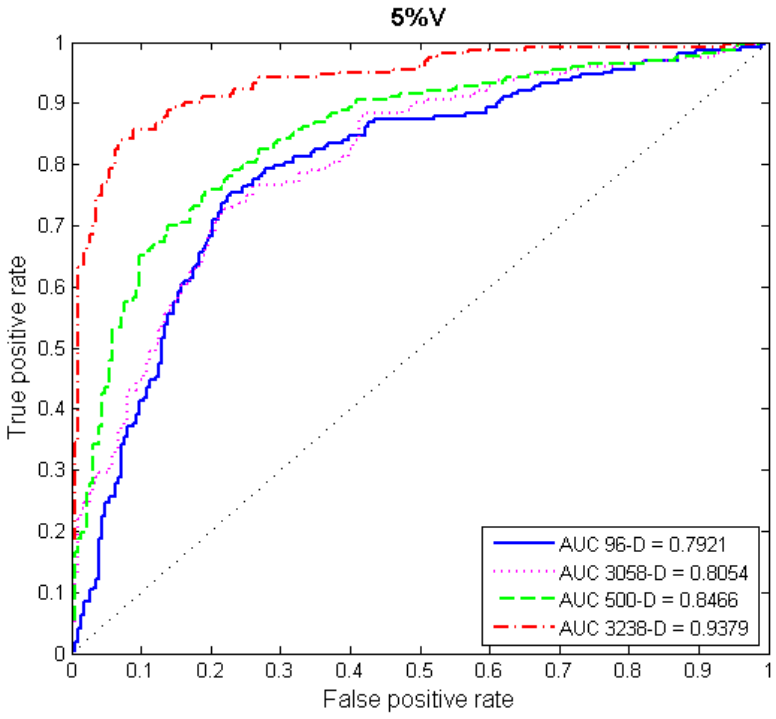

(b)

Figure 4.4 ROCs of proposed 3238-D feature model and other compared methods on detecting seam carving with carving rate as 5%.

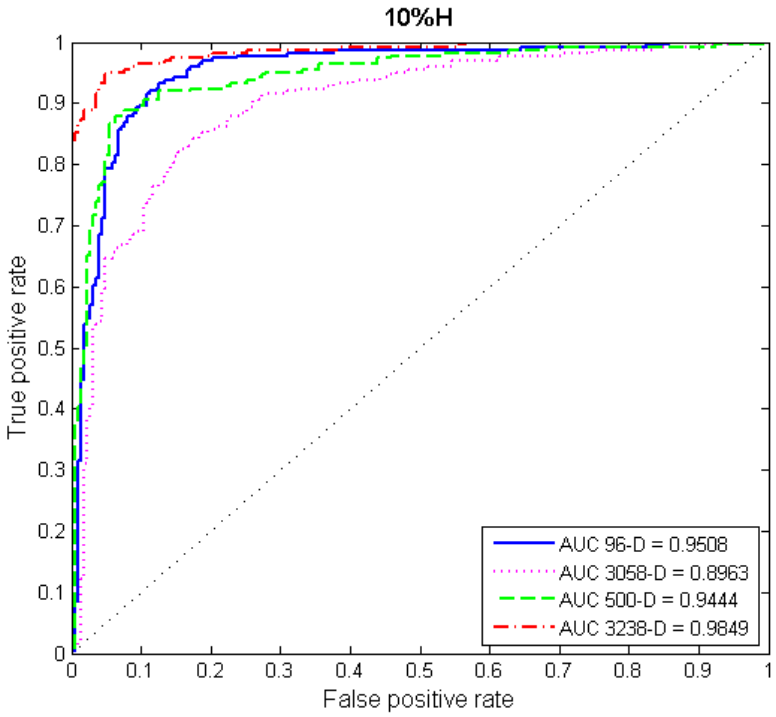

(a)

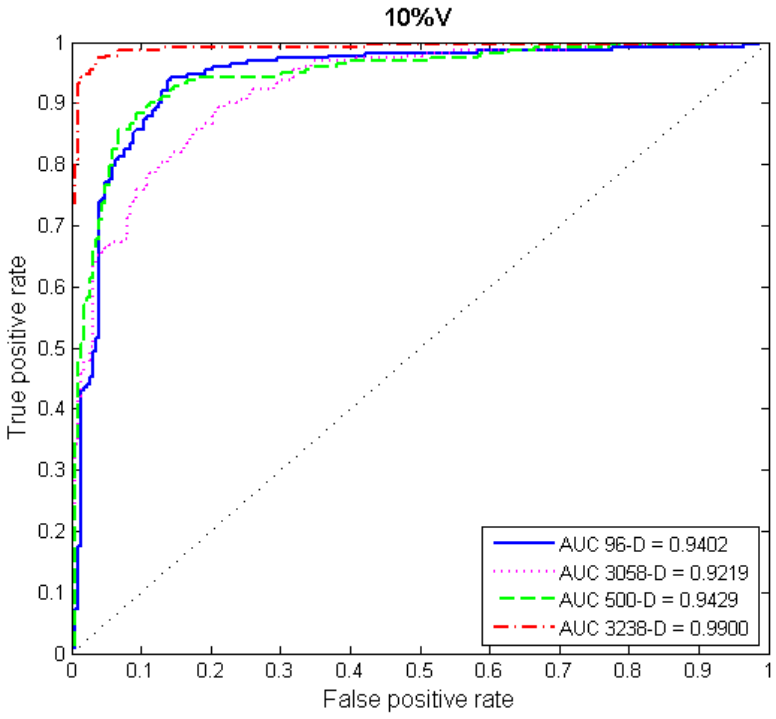

(b)

Figure 4.5 ROCs of proposed 3238-D feature model and other compared methods on detecting seam carving with carving rate as 10%.

4.3 Conclusion and Discussion

In this chapter, an advanced model is designed to further improve the performance of the state-of-the art on detecting the process of seam carving applied to digital images at low carving rate. In order to catch the imperceptible traces left by low carving rate seam carving, a 3258-D feature vector is proposed, in which 3028 features are adopted to capture the changes of relationship between neighboring pixels, and 180 features are utilized for detecting the changes of energy distribution. Based on the conducted experimental works, the average accuracies of detecting a carving rate as 5% or 10% has been boosted from 76.67% (achieved by the 3058-D model) and 88.88% (achieved by the 96-D model) to 85.75% and 94.87%. Although it has been observed that overfitting is more significant when the feature model is more complex, the performance of the proposed 3258-D model is still better than the state-of-the-art on most of the designed seam carving scenarios. The possible way to further improve the proposed 3258-D model and to reduce overfitting is to utilize advanced feature reduction techniques, such as SVM-RFE, and it is very likely to be succeeded based on experiences as presented in Chapter 3.

CHAPTER 5

A CONVOLUTIONAL NEURAL NETWORK DESIGNED FOR SEAM CARVING DETECTIION

As introduced in previous chapters, forensic research of detecting seam carving is kept pushing forward. However, most of the existing methods designed for seam carving detection, including the three methods presented in this dissertation, focus on feature engineering; and classifiers have been applied to map the features to class labels to ensure better performance, as shown in Figure 5.1. Although the detection accuracy has been boosted significantly since this forensic subject was addressed, the optimal performance is undoubtedly restricted by the handcrafted features. Therefore, a system with more machine self-learning and less manual feature designing is assumed to have better performance than conventional method. Inspired by the tremendous success achieved by deep learning on computer vision and image forensics, a deep learning framework, more specifically, a deep convolutional neural network (CNN) based framework, is proposed in this chapter to detect seam carving applied to digital images. Unlike the existing seam carving detection methods, whose feature extraction and pattern classification are two separate procedures, the proposed CNN-based deep learning architecture jointly optimizes these two procedures. In

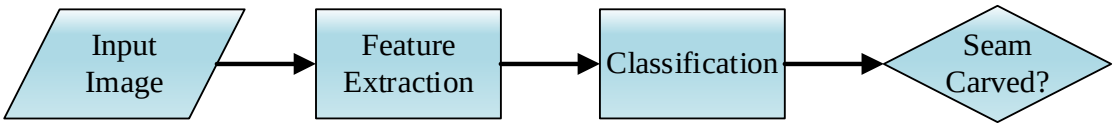

Figure 5.1 General framework of exiting blind passive forensic methods for seam carving detection.

the designed architecture, six convolutional modules are employed to reveal the traces left by the process of seam carving, and a pre-processing layer is adopted to further improve the performance. The experiments conducted on a large dataset have demonstrated that, compared with the current state-of-the-art, our CNN-based method significantly boosts the classification accuracies at the medium and low seam carving rates, and retains near-to-perfect classification performance at high seam carving rates.

5.1 Background of Deep CNN

In 1989, a neural network named ‘Net-5’ was designed for a designed handwritten digit recognition problem [51]. The idea behind this structure is based on two major concerns: reducing the number of free parameters to gain better generalization, and forcing hidden units to learn from local information to achieve better results. The hidden layers in the Net-5 are composed of numbers of feature maps, while each unit in one feature map is connected to units within a size fixed neighbourhood, for instance 3×3, on the input plane. Therefore, the number of free parameters is largely reduced comparing with traditional fully connected neural networks. Furthermore, weight sharing strategy is applied that is all units in a feature map share the same set of weights, and subsampling is utilized as well to reduce the complexity of the network. Thus, much less parameters are considered during the computation. Besides, back propagation technique [52] is also employed to train the neural network. According to the reported results, Net-5 has achieved the best performance among five compared structures. Noted, Net-5 is the first CNN as known and the idea behind is still the essence of today’s various deep CNNs. Later in [53], the above introduced work was applied on recognizing handwritten digits taken by U.S. Mail, and

the network has been extended from Net-5's two hidden layers to three hidden layers, including two convolutional layers, and one fully connected layer. Although the number of convolutional layer was not increased, the number of kernels adopted, that is the set of in each hidden layer are significantly increased. The results turned out to be the state of the art. In [54], another CNN named 'LeNet-5' is proposed for handwritten character recognition. However, the network is still shallow. The first deep CNN architecture called 'AlexNet' was presented in 2012 [55]. This network has achieved remarkable success in the ILSVRC-2012 competition which is considered as a huge step to the machine learning society. In 'AlexNet', five convolutional layer are employed to generate hierarchical feature maps. Besides, max-pooling is applied to reduce the size of the network. To increase non-linearity, ReLU is utilized in 'AlexNet' as well. Finally, 'AlexNet' achieved a top-5 test error rate of 15.3% on the ImageNet database [56] while the second-best result was 26.2%.

After the big success of 'AlexNet', deep CNN has aroused tremendous interests and several successful CNNs have been presented for image classification, such as 'ZF Net' [57], 'VGGNet' [58], 'GoogLeNet' [59], 'ResNet' [60], etc. Not only the research of image classification, deep CNN has been widely spread to other related areas and achieved successes, such as face recognition, human action recognition, and steganalysis [61-63] as well.

By reviewing the proposed CNNs, most of the networks are based on a similar structure that is a hierarchical architecture starts with multiple stages of convolutional modules and ends with a classification module. A common convolutional module includes a convolutional layer, an activation layer, and a pooling layer. The convolutional layer is a

trainable filter bank which can be considered as a feature extractor. The activation layer brings non-linearity to the network. The pooling layer reduces the quantity of features extracted from immediately prior convolutional layer to avoid overfitting. By stacking a series of convolutional modules, hierarchical feature maps are extracted and then fed into the classification module composed of one or more fully-connected layers, and the softmax layer with cross-entropy loss. Through back-propagation, weights and biases in convolutional layers will be optimized so as to reduce the training loss, and the power of the network will then be enforced to predict the labels of unseen data.

5.2 Proposed Deep CNN

The overall architecture of the proposed CNN is illustrated in Figure 5.2. Instead of directly feeding the original images into the networks, a high-pass filtering (HPF) layer with kernel size of 5×5×1 [61-63] (height × width × number of input feature maps) is employed to pre-process input images. The reasons of doing so are: 1) The operation of seam carving will delete low energy seams from the image which could generate slightly but somehow different textures. Therefore, the discriminative information carried by the original image could be amplified by the high-pass filtering; 2) According to our conducted experiments, the performance of the deep CNNs decreases significantly while HPF layer is excluded. Based on these consideration, HPF layer has been employed as pre-processing in our proposed deep CNN architecture.

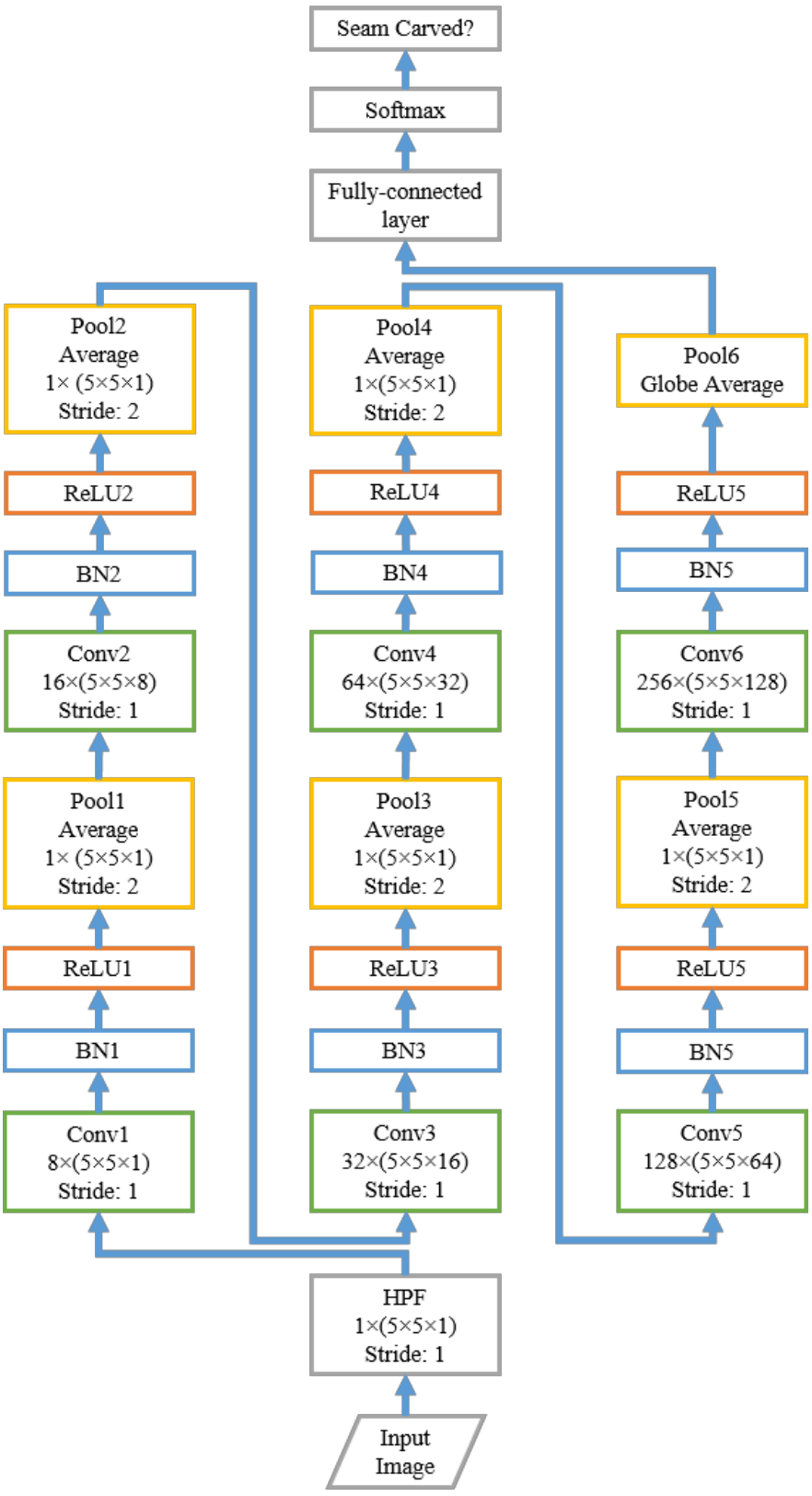

Figure 5.2 The proposed CNN architecture. Parametric setting of each layer is included in the corresponding box.

Following the HPF layer is the CNN hierarchical structure which consists of six convolutional modules and one fully-connected linear classification module. In the first convolutional layer (Conv1), the input, i.e., the pre-processed input image, is to be filtered by 8 kernels of size 3×3×1 each. In the following convolutional layers (Conv2 – Conv6), there are 16 kernels of size 3×3×8 in Conv2, 32 kernels of size 3×3×16 in Conv3, 64 kernels of size 3×3×32 in Conv4, 128 kernels of size 3×3×64 in Conv5 and 256 kernels of size 3×3×128 in Conv6, respectively, so as to generate hierarchical feature maps.

Different from the introduced conventional CNN module, an additional layer, called batch normalization (BN) layer [64], is employed between each convolutional layer and the following activation layer. As the outputs generated by the convolutional layer are normalized by the corresponding BN layer, the so called 'internal covariate shift' [64] is reduced which helps to accelerate the training speed and to reduce the influence caused by poor initialization.

To increase the non-linearity of the proposed deep architecture, rectified linear units (*ReLU*) are served as the non-linear activation functions in each of the convolutional modules, as shown in Figure 5.3. Comparing with other popular non-linear functions, such as hyperbolic tangent and Sigmoid, *ReLU* has relatively simple form, i.e., gradient is 1 for positive inputs and 0 for negative inputs. Such characteristics could accelerate the speed on training deep neural networks, and also avoid the vanishing of gradient happens during the training stage [65].

As the process of seam carving is to remove lower energy pixels, those higher energy pixels which normally have large intensity value are more likely remained in the image. Because of this characteristics, focusing on the maximum pixel value of a local

region, which is normally considered in computer vision, is intuitively insufficient to discover the trace of seam carving. Therefore, average pooling is employed in the proposed deep CNN framework for spatial sub-sampling instead of max pooling popularly utilized in computer vision. In the last pooling layer, namely, in Pool6, the kernel size for pooling is fixed to the spatial size of the input feature maps. Therefore, each input feature map will be aggregated to one single number, which serves as a feature for the classification. As 256 feature maps are inputted into pool6, 256 features are generated and fed into the fully-connected linear classification module for each image.

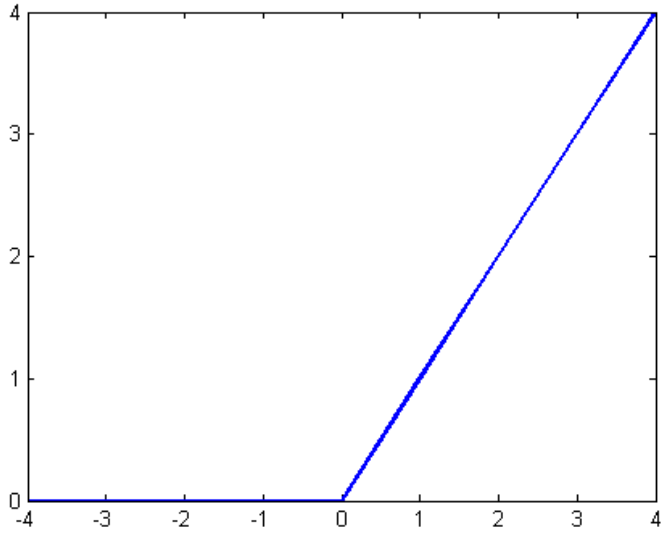

$$ReLU(x) = \begin{cases} 0, & x \leq 0 \\ x, & x > 0 \end{cases}$$

Figure 5.3 Rectified linear unit (ReLU).

5.3 Experimental Results

In this work, we also implemented the seam carving algorithm [29] in MATLAB and established 12 seam carved image sets using the BOSSbase v1.01 [66], a well-established image database to benchmark steganography and steganalysis algorithms. It contains 10,000 never-compressed grayscale images with the size of 512×512. For each image in the BOSSbase, the seam carving algorithm reduced the image height by 5%, 10%, 20%, 30%, 40% and 50%, respectively. Similarly, by scaling the width in the same manner, totally 12 different seam carved images were obtained for each image in the BOSSBase. Therefore, 12 seam carved sets were created and each contains 10,000 seam carved images, denoted as '5%H', '10%H', '20%H', '30%H', '40%H', '50%H', '5%V', '10%V', '20%V', '30%V', '40%V', and '50%V', respectively. To evaluate the performance of the proposed CNN architecture, the experiments were conducted to detect the 12 designed seam carving cases.

In the experiments, the proposed CNN architecture was implemented using the Caffe toolbox [67], and stochastic gradient descent was applied to train all the CNNs with the batchsize of 64 images. We fixed the momentum as 0.9 and the weight decay as 0.0005. The learning rate was initialized to 0.001 and forced to decrease 10% after each 5000 iterations. To fairly compare the performance with the state-of-the-art, we not only implemented and tested methods proposed by Ryu et al. [40] and Yin et al. [41], but also examined the performance of the 3238-D feature model which has been proposed in Chapter 4. Each of the three compared methods was tested on the 12 seam carving cases with linear SVM as the classifier [46]. Additionally, 2-fold cross validation was applied throughout the experiments.

As shown in Table 4.1, the proposed CNN architecture performs significantly better than the two state-of-the-art of seam carving detection when the scaling rate is below 30%. In particularly, our method achieves 90% and 93% detection accuracies when testing '5%H' and '5%V', which is 20% higher than the performance achieved by Ryu et al.'s and Yin et al.'s methods. It is also observed that the 3238-D model outperforms the on those low carving rate cases although it still underperforms the proposed deep CNNs. Notably, the detection accuracy increases monotonically with the carving rate for all tested methods, and the gap between the proposed method and the tested prior arts is getting smaller as well. The reason behind is that, overfitting is more significant for the methods which are more complicated and more powerful on modelling, such as proposed deep CNN and 3238-D as well, on detecting easy cases, i.e., detecting images in which a large amount of seams are carved out. Performance of the proposed CNN architecture without the HPF layer is also investigated. As illustrated in Figure 5.4, the detection accuracy is dramatically boosted by employing the HPF layer, particularly for seam carved images at low carving rate, such as '5%H' and '5%V'. Furthermore, performance of the proposed CNN with a fixed kernel size as 3×3 or 7×7 for all included convolutional layers are investigated, respectively. As observed from Figures 5.5, 5.6, 5.7, and 5.8, by setting kernel size as 7×7, the CNN has achieved the lowest training loss than other four configurations. However, the proposed CNN, in which kernel size for all convolutional layers is set as 5×5, achieves equal or lower error rates than 7×7 in the testing. Moreover, the larger the kernel size is, the more complex the deep CNN is to be, and more computational resources are needed. Therefore, kernel size as 5×5 is applied to each convolutional layers in the proposed CNN.

In Figures 5.9, 5.10, and 5.11, three samples are presented, and the feature maps learnt by the proposed deep CNNs are visualized as heat maps. The larger the value is in the heat map, the more suspicious the region is It is observed that the trained deep neural network can effectively discover the region where the seams are deleted, by learning from the seam carved copies, while irrelevant regions are learnt from the non-seam carved images. This has also illustrated the effectiveness of the proposed CNN architecture on detecting seam carving.

Table 5.1 Average Detection Accuracy of Proposed CNN versus the State-of-the-Art.

	5%H	10%H	20%H	30%H	40%H	50%H
Ryu et al.	65.92%	72.88%	82.78%	90.31%	95.01%	97.77%
Yin et al.	70.26%	83.60%	94.35%	97.90%	99.16%	**99.71%**
3238-D	85.23%	92.29%	96.22%	97.84%	98.51%	98.99%
CNN	**90.37%**	**95.18%**	**97.84%**	**98.76%**	**99.21%**	99.56%

	5%V	10%V	20%V	30%V	40%V	50%V
Ryu et al.	71.13%	79.83%	88.36%	93.18%	96.08%	97.79%
Yin et al.	58.74%	71.50%	85.68%	93.31%	97.25%	98.97%
3238-D	86.10%	93.64%	97.50%	98.74%	99.24%	99.52%
CNN	**93.99%**	**96.71%**	**98.55%**	**99.08%**	**99.45%**	**99.60%**

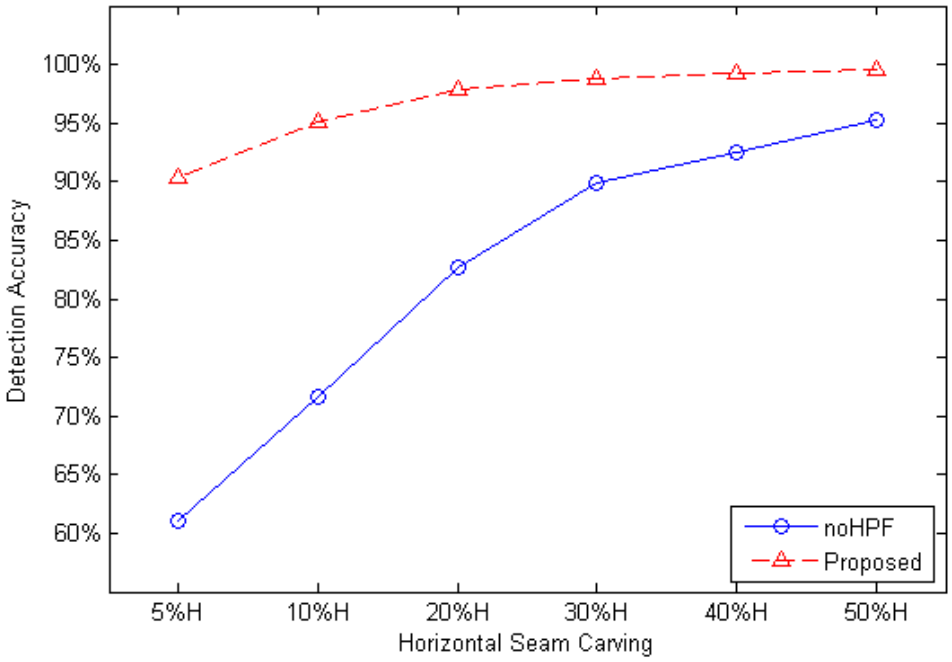

(a)

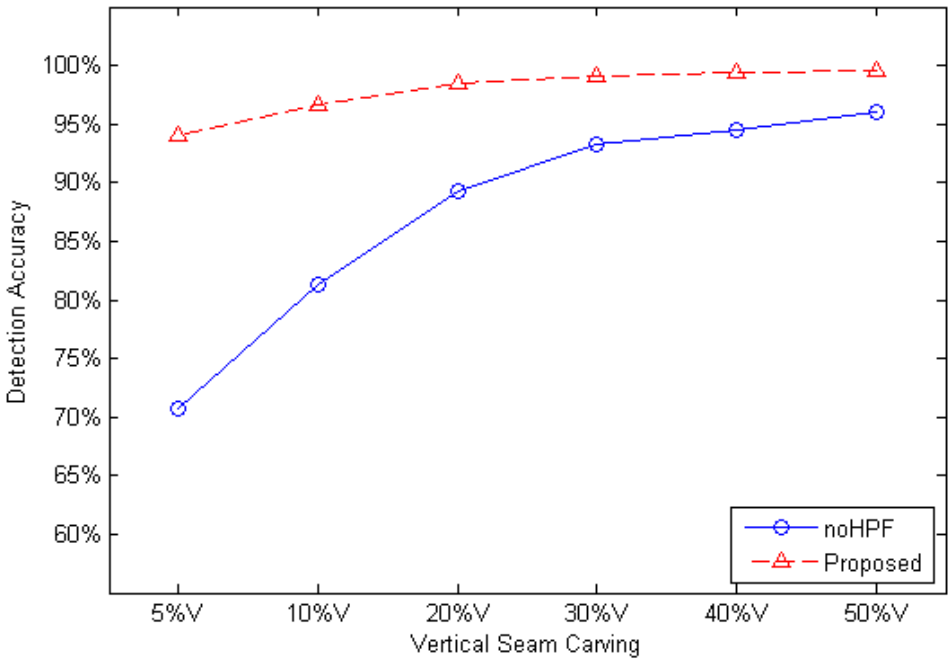

(b)

Figure 5.4 Performance of proposed CNN versus the similar architecture without HPF layer (noHPF) on detecting 12 seam carving scenarios.

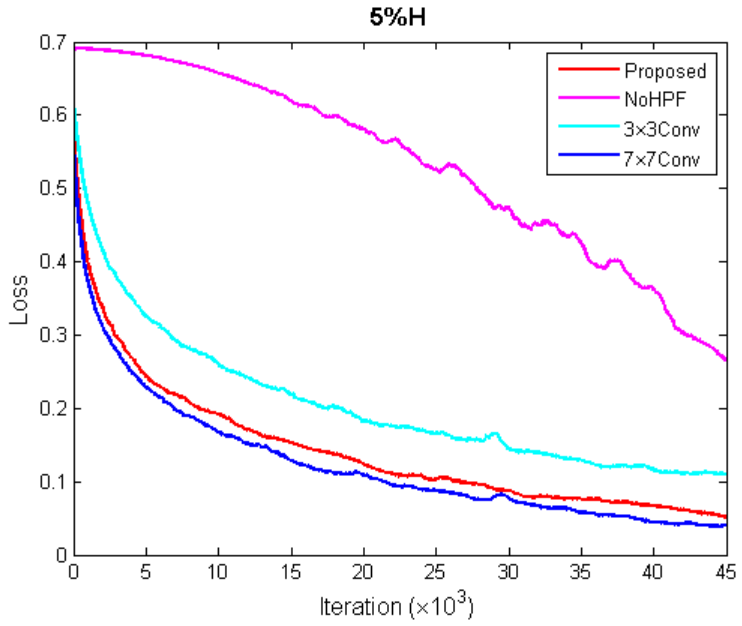

(a)

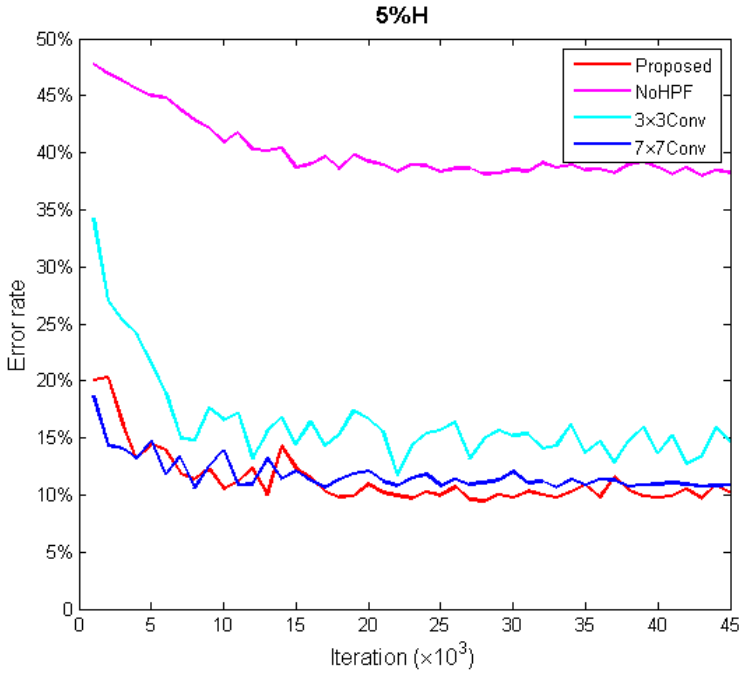

(b)

Figure 5.5 Training loss and testing error rate of four compared architectures on detecting horizontal seam carving with carving rate as 5%.

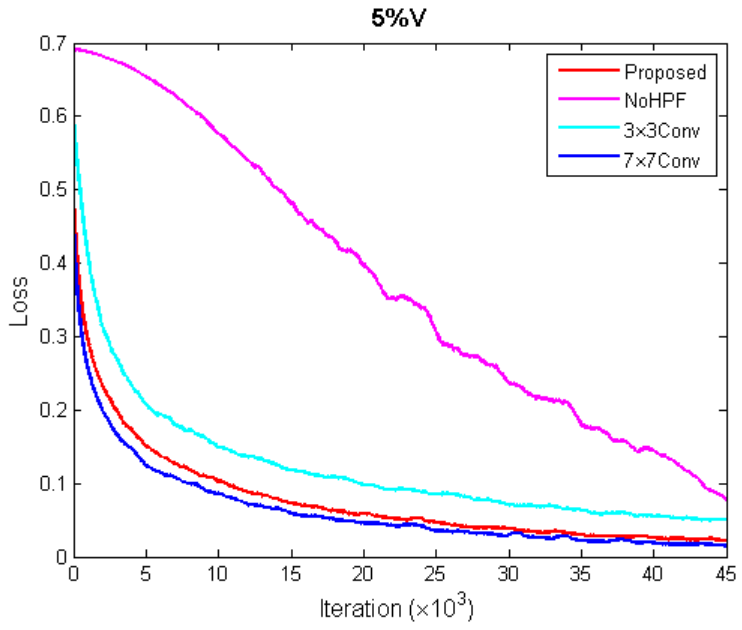

(a)

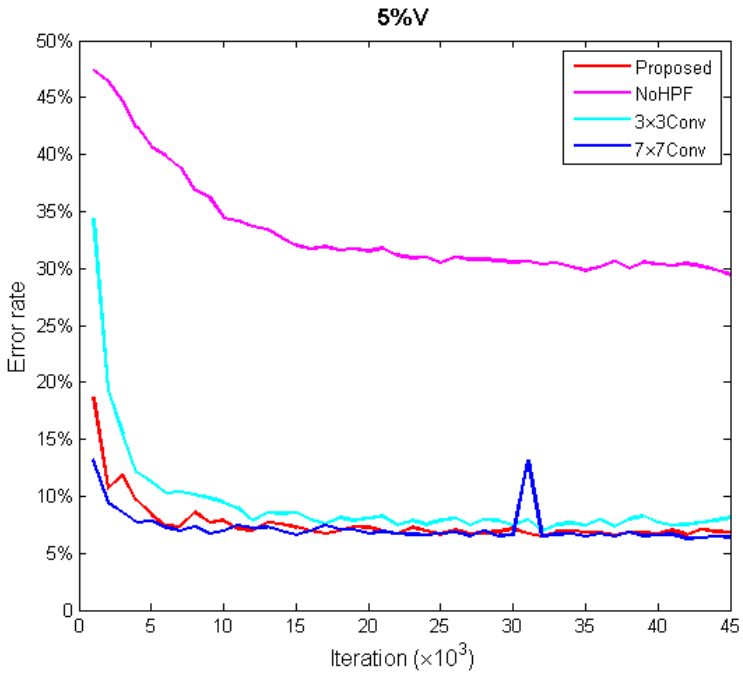

(b)

Figure 5.6 Training loss and testing error rate of four compared architectures on detecting vertical seam carving with carving rate as 5%.

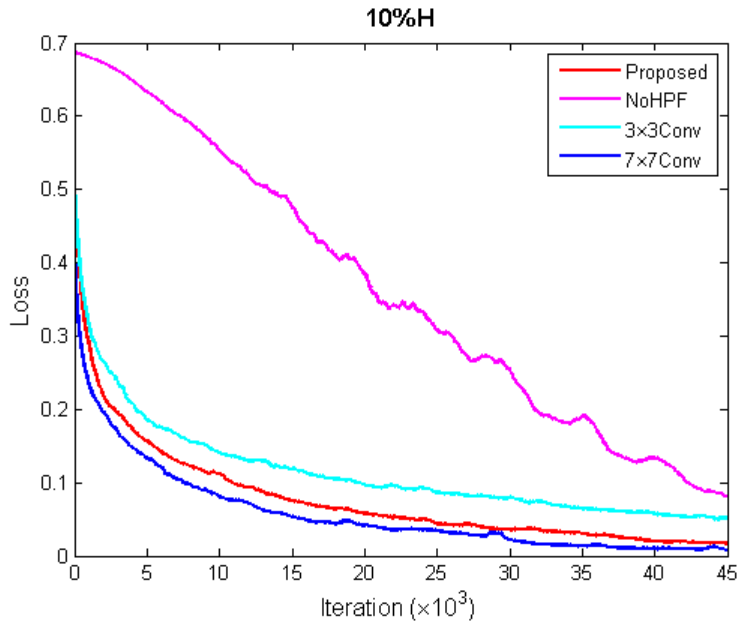

(a)

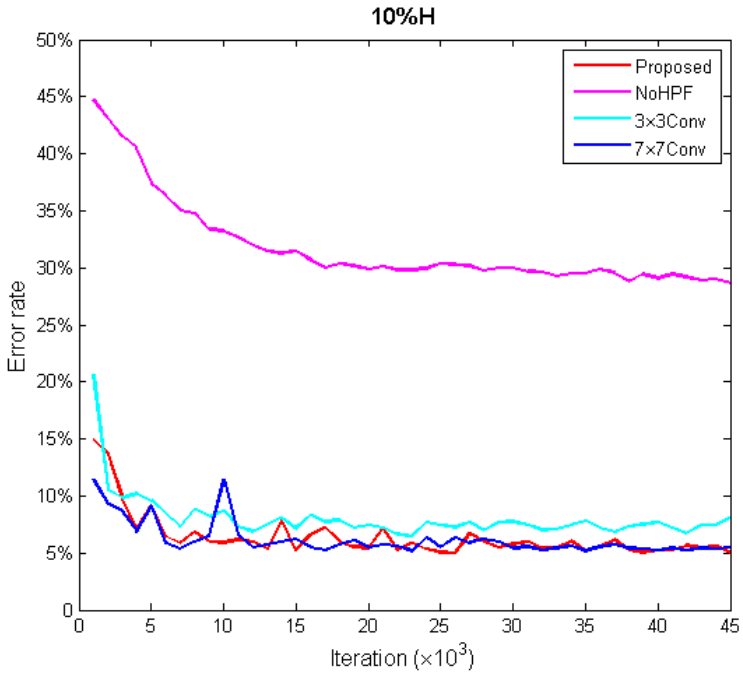

(b)

Figure 5.7 Training loss and testing error rate of four compared architectures on detecting horizontal seam carving with carving rate as 10%.

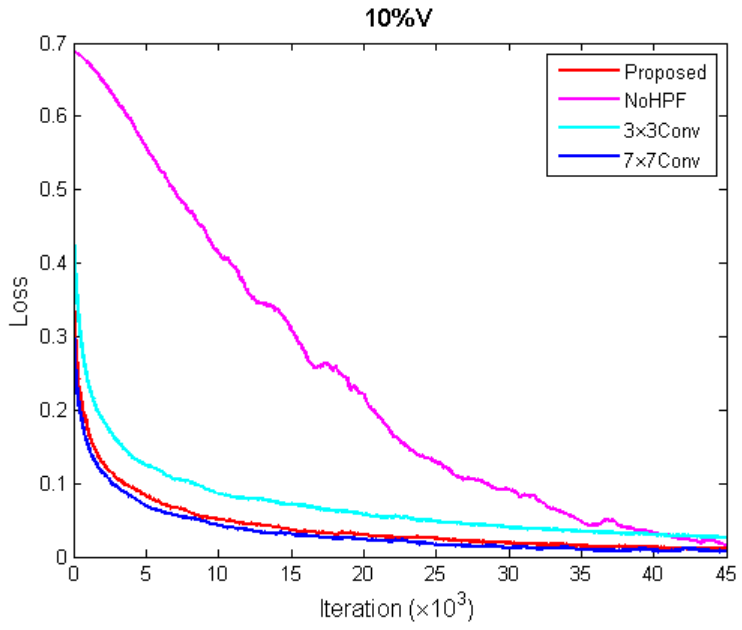

(a)

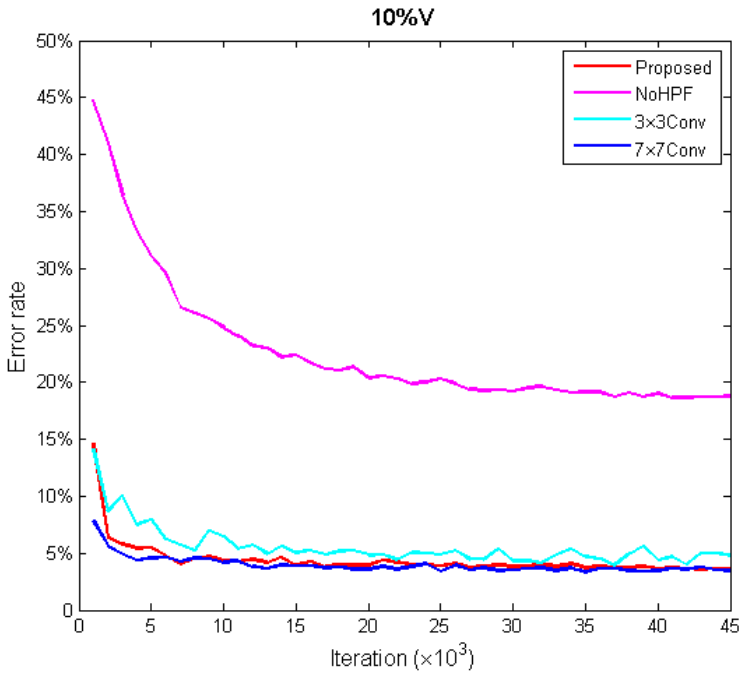

(b)

Figure 5.8 Training loss and testing error rate of four compared architectures on detecting vertical seam carving with carving rate as 10%.

(a)

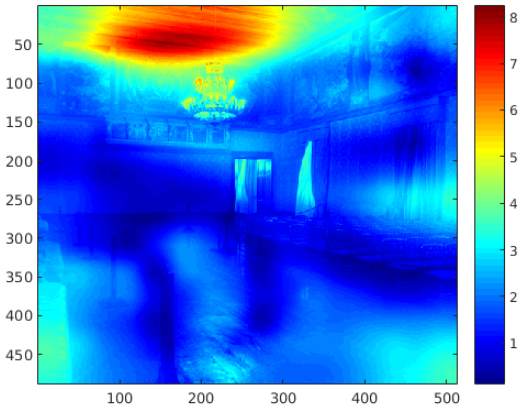

(b)

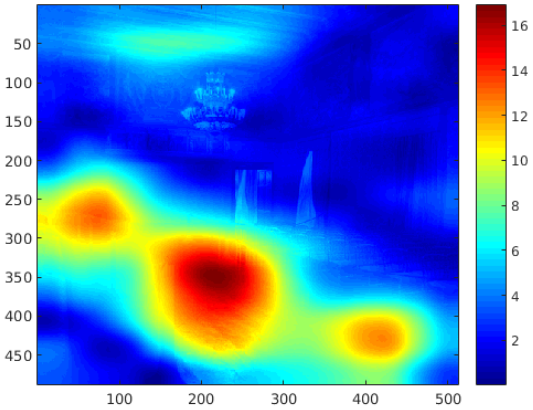

(c)

Figure 5.9 (a) The ground truth of carved seams shown in the original sample image with carving rate as 5%; (b) The heat map learnt from the original non-seam carved image; (c) The heart map learnt from the seam carved copy.

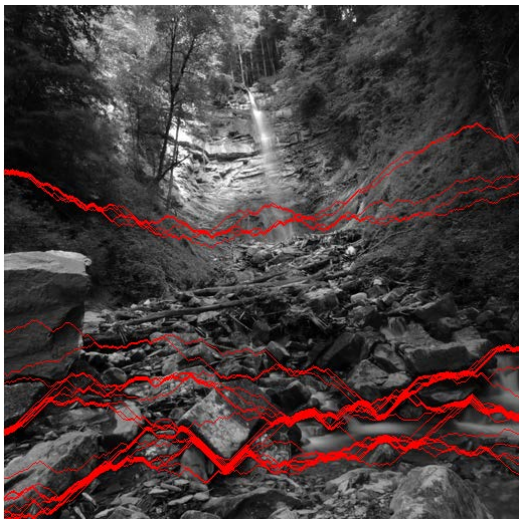

(a)

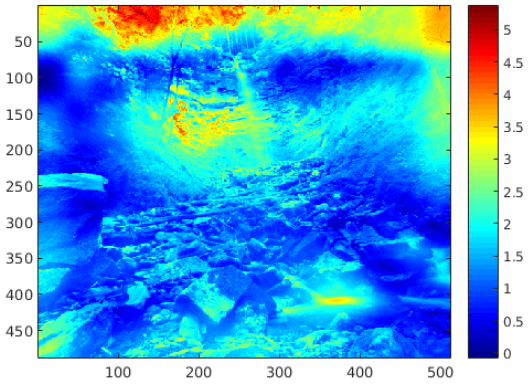

(b)

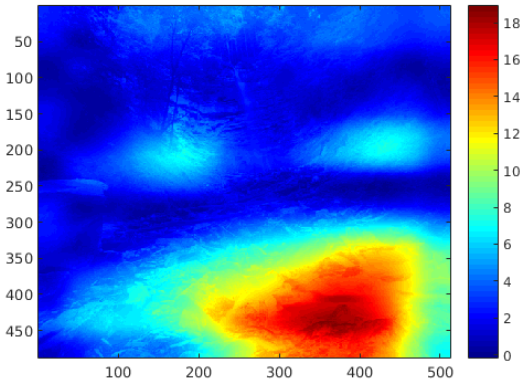

(c)

Figure 5.10 (a) The ground truth of carved seams shown in the original sample image with carving rate as 5%; (b) The heat map learnt from the original non-seam carved image; (c) The heart map learnt from the seam carved copy.

(a)

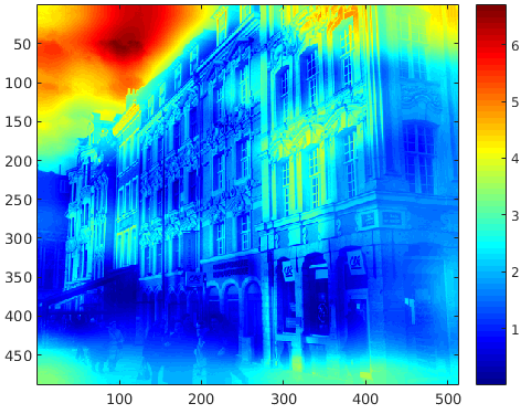

(b)

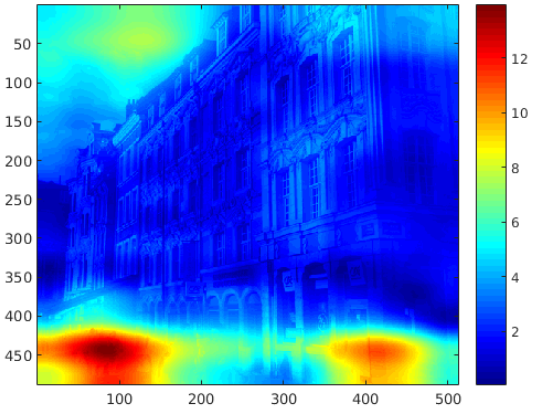

(c)

Figure 5.11 (a)The ground truth of carved seams shown in the original sample image with carving rate as 5%; (b) The heat map learnt from the original non-seam carved image; (c) The heart map learnt from the seam carved copy.

5.4 Conclusion

In this chapter, a convolutional neural network architecture has been described and utilized for seam carving detection. It is the first deep learning framework on this research topic as far as we know. Indicated by experimental results, the proposed deep learning method can successfully detect seam carving in uncompressed digital images, and outperform the state-of-the-art in most of the experiments. In particular, the proposed deep convolutional neural network has achieved remarkable performance on detecting low carving rate cases, i.e., 5% and 10% carving rate cases. However, it should be also noticed that the proposed deep CNN could underperform the prior arts on detecting seam carving with extremely high carving rate due to the overfitting, and the performance of deep neural network on detecting seam carving in compressed images, i.e., JPEG images, needs to be further investigated. Therefore, the future work will be focusing on the remaining questions. Overall, through our work, it has been shown that deep learning could be a new direction for the forensic research of seam carving detection, and it could be far more successful than we have achieved.

CHAPTER 6

SUMMARY

6.1 Contributions

The contributions of this dissertation can be concluded as follows.

1. Four passive blind forensic methods have been proposed for seam carving detection, and the performance achieved by the current state-of-the-art in this area has been successively improved. Especially the accuracies in detecting seam carved images with a carving rate as 5% or 10%, which are most difficult for seam carving can now be successfully detected.

2. The local derivative pattern (LDP) has been firstly introduced to this forensic research. The remarkable performance has been achieved in the comprehensive experimental works. They are reported in Chapters 2, 3, and 4 respectively, which have indicated that the effectiveness and potential of LDP on detecting seam carving.

3. Support vector machine based recursive feature elimination (SVM-RFE) is firstly applied for feature selection in the research on seam carving detection. With the 500 features selected by using SVM-RFE, the performance achieved by the proposed 3058-D feature model has been significantly improved.

4. The deep neural network, specifically deep convolutional neural network, has been designed for and utilized to detect seam carving. The experimental results have indicated that the deep learning technologies could be the ultimate solution for this forensic research.

6.2 Discussion and Future Works

From the first three pieces of the proposed works, it can be concluded that a hand designed feature model comprised of various types of advanced features could have better performance than any individual on detecting seam carving with low carving rate. It is because the difference between un-seam carved images and seam carved images at low carving rate is almost imperceptible which makes these two classes of images extremely hard to be separated. Thus, a more powerful feature model, generally to be complex, could

have more chance to perform better than a less complex feature model on detecting such difficult seam carving scenarios. It should also be noticed that, more significant overfitting is a potential weakness of complex feature models. Although the detection accuracies achieved on UCID database has been improved significantly by this dissertation research, it is believed that the performance on detecting low carving rate seam carving can be further improved. Therefore, to design a more advanced feature model which has better overall performance could be an important future work in this field.

In Chapter 5, a deep learning based method, specifically a convolutional neural network based architecture, has been proposed for detecting seam carving applied to uncompressed images. This is the first piece of work which has successfully applied deep learning to this forensic topic. However, due to the limited computational resources, the design of the deep network is somehow constrained. Hence, it is believed that the potential of this novel technique on seam carving detection has not been fully discovered yet. Modifications, such as increasing the depth of the CNN, increasing the channels of each convolutional layer, enlarging the size of receptive field, could all possibly enhance the current network, and these could be future research works.

Although a few results have been reported in Chapter 3 for detecting seam carving applied to JPEG images, the research work of seam carving detection in JPEG domain that has been done in this dissertation is far from enough. As JPEG is widely utilized nowadays, it is important to provide robust and efficient forensic techniques to detect seam carving applied to JPEG images. This should be addressed in the future research.

REFERENCES

[1] H. Farid, "A survey of image forgery detection," *IEEE Signal Process. Mag.*, vol 26, no. 2, pp. 16-25, 2009.

[2] A. Piva, "An overview on image forensics," *ISRN Signal Process.*, vol. 2013, Article ID 496701, 2013.

[3] H. Farid, "Photo forensics," Cambridge, MA: MIT Press, 2016.

[4] Z. J. Geradts, J. Bijhold, M. Kieft, K. Kurosawa, K. Kuroki, and N. Saitoh, "Methods for identification of images acquired with digital cameras," *Proc. SPIE Enabling Technologies for Law Enforcement and Security*, vol. 4232, pp. 505-512, 2001.

[5] M. Kharrazi, H. T. Sencar, and N. Memon, "Blind source camera identification," *IEEE Int. Conf. on Image Process.*, pp. 709-712, 2004.

[6] S. Bayram, H. T. Sencar, N. Memon, and I. Avcibas, "Source camera identification based on CFA interpolation," *IEEE Int. Conf. on Image Process.*, vol. 3, pp. 69-72, 2005.

[7] J. Lukáš, J. Fridrich, and M. Goljan, "Determining digital image origin using sensor imperfections," *Image and Video Communications and Process.*, vol. 5685, pp. 16-20, 2005.

[8] S. Bayram, H. T. Sencar, and N. Memon, "Improvements on source camera model identification based on CFA interpolation," *Proc. IFIP WG 11.9 Int. Conf. Digital Forensics*, Orlando, FL, pp. 24-27, 2006.

[9] Y. Long and Y. Huang, "Image based source camera identification using demosaicking," *IEEE Int. Workshop on Multimedia Signal Process.*, vol. 3, 2006.

[10] A. J. Fridrich, B. D. Soukal, and A. J. Lukáš, "Detection of copy-move forgery in digital images," *Proc. Digit. Forensic Res. Workshop*, 2003.

[11] W. Luo, J. Huang, and G. Qiu, "Robust detection of region-duplication forgery in digital image," *Proc. 18th Int. Conf. Pattern Recognit. (ICPR)*, vol. 4, pp. 746-749, 2006.

[12] S. Bayram, H. T. Sencar, and N. Memon, "An efficient and robust method for detecting copy-move forgery," *Proc. IEEE Int. Conf. Acoust. Speech Signal Process. (ICASSP)*, pp. 1053-1056, Apr. 2009.

[13] S. Bravo-Solorio and A. K. Nandi, "Exposing duplicated regions affected by reflection rotation and scaling," *Proc. IEEE Int. Conf. Acoust. Speech Signal Process. (ICASSP)*, pp. 1880-1883, May. 2011.

[14] S.-J. Ryu, M. Kirchner, M.-J. Lee, and H.-K. Lee, "Rotation invariant localization of duplicated image regions based on Zernike moments," *IEEE Trans. Inf. Forensics Security*, vol. 8, no. 8, pp. 1355-1370, Aug. 2013.

[15] J. Lukáš and J. Fridrich, "Estimation of primary quantization matrix in double compressed JPEG images," *Proc. Digit. Forensic Res. Workshop*, pp. 5-8, 2003.

[16] A. C. Popescu and H. Farid, "Statistical tools for digital forensics," *Proc. 6th Int. Workshop Inf. Hiding*, pp. 128-147, 2004.

[17] D. Fu, Y. Q. Shi, and W. Su, "A generalized Benford's law for JPEG coefficients and its applications in image forensics," *Proc. SPIE Electronic Imaging Security and Watermarking of Multimedia Contents IX*, vol. 6505, pp. 1L1-1L11, Feb. 2007.

[18] B. Li, Y. Q. Shi, and J. Huang, "Detecting doubly compressed JPEG images by using mode based first digit features," *Proc. IEEE Int. Workshop Multimedia Signal Process.*, pp. 730-735, Oct. 2008.

[19] F. Huang, J. Huang, and Y. Q. Shi, "Detecting double JPEG compression with the same quantization matrix," *IEEE Trans. Inf. Forensics Security*, vol. 5, no. 4, pp. 848-856, Dec. 2010.

[20] V. Athitsos, M. J. Swain, and C. Frankel, "Distinguishing photo-graphs and graphics on the World Wide Web," *Proc. Workshop on Content-Based Access of Image and Video Libraries (CBAIVL '97)*, 1997.

[21] H. Farid and S. Lyu, "Higher-order wavelet statistics and their application to digital forensics," *IEEE Workshop on Statistical Analysis in Comput. Vision (in conjunction with CVPR)*, Madison, Wisconsin, 2003.

[22] T.-t. Ng and S.-f. Chang, "Classifying photographic and photo-realistic computer graphic images using natural image statistics," *ADVENT Technical Report*, Columbia University, 2004.

[23] S. Dehnie, T. Sencar, and N. Memon, "Digital image forensics for identifying computer generated and digital camera images," *IEEE Int. Conf. on Image Process.*, Atlanta, GA, pp. 2313-2316, 2006.

[24] W. Chen, Y. Q. Shi, and G. Xuan, "Identifying computer graphics using hsv color model and statistical moments of characteristic func-tions," *IEEE Int. Conf. on Multimedia and Expo.*, Beijing, China, pp. 1123-1126, 2007.

[25] W. Chen, Y. Shi, G. Xuan, and W. Su, "Computer graphics identification using genetic algorithm," *19th Int. Conf. on Pattern Recog. (ICPR)*, December 8-11, Tampa, Florida, USA, 2009, pp. 1-4, 2008.

[26] P. Sutthiwan, J. Ye, and Y. Shi, "An enhanced statistical approach to identifying photorealistic images," *Proc. 8th Int. Workshop Digital Forensics and Watermarking*, pp. 323-335, 2009.

[27] Z. Li, J. Ye, and Y. Shi, "Distinguishing computer graphics from photo-graphic images using local binary patterns," *Proc. 11th Int. Workshop on Digital Forensics and Watermarking*, 2012.

[28] J. Wang, T. Li, Y. Q. Shi, S. Lian, and J. Ye, "Forensics feature analysis in quaternion wavelet domain for distinguishing photographic images and computer graphics," *Multimedia Tools Appl.*, DOI: 10.1007/s11042-016-4153-0, 2016.

[29] S. Avidan and A. Shamir, "Seam carving for content-aware image resizing," *ACM Trans. Graphics*, vol.26, no.3, July 2007.

[30] A.Sarkar, L. Nataraj, and B. S. Manjunath, "Detection of seam carving and l ocalization of seam insertions in digital images," *Proc. 11th ACM Workshop on Multimedia and Security (MM&Sec'09)*, New York, NY, USA, pp. 107-116, 2009.

[31] Y. Q. Shi, C. Chen, and W. Chen, "A Markov process based approach to effective attacking JPEG steganography," *Proc. 8th Inf. Hiding Workshop*, pp. 249-264, 2006.

[32] C. Fillion and G. Sharma, "Detecting content adaptive scaling of images for forensic applications," *Media Forensics and Security, SPIE Proc.*, p. 75410, 2010.

[33] W. Chang, T. K. Shih, and H. Hsu, "Detection of seam carving in JPEG images," *Proc. iCAST-UMEDIA*, 2013.

[34] K. Wattanachote, T. K. Shih, W. Chang, and H. Chang, "Tamper detection of JPEG image due to seam modification," *IEEE Trans. Inf. Forensics and Security*, vol. 10, no. 12, pp. 2477-2491, 2015.

[35] Q. Liu and Z. Chen, "Improved approaches with calibrated neighboring joint density to steganalysis and seam-carved forgery detection in JPEG images," *ACM Trans. Intell. Syst. and Technol.*, vol. 5, no. 4, 2014.

[36] J. Fridrich and J. Kodovsky, "Rich models for steganalysis of digital images," *IEEE Trans. on Inf. Forensics and Security*, 2012.

[37] Q. Liu, "Exposing seam carving forgery under recompression attacks by hybrid large feature mining," *23rd Int. Conf. on Pattern Recog. (ICPR)*, pp. 1036-1041, 2016.

[38] Q. Liu, "An approach to detecting JPEG down-recompression and seam carving forgery under recompression anti-forensics," *Pattern Recog.*, vol. 65, pp. 35-46, 2016.

[39] J. Wei, Y. Lin, and Y. Wu, "A patch analysis method to detect seam carved images," *Pattern Recog. Lett.*, vol. 36, pp. 100 -106, 2014.

[40] S. Ryu, H. Lee, and H. Lee, "Detecting trace of seam carving for forensic analysis," *IEICE Trans. Inf. and Systems*, vol. E97-D, no. 5, pp. 1304-1311, 2014.

[41] T. Yin, G. Yang, L. Li, D. Zhang, and X. Sun, "Detecting seam carving based image resizing using local binary patterns," *Comput. Security*, vol. 55, pp. 130-141, 2015.

[42] T. Ojala, M. Pietikäinen, and D. Harwood, "A comparative study of texture measures with classification based on feature distributions," *Pattern Recog.*, vol. 29, no. 1, pp. 51-59, 1996.

[43] W. Lu and M. Wu, "Seam carving estimation using forensic hash," *Proc. 13th ACM Multimedia Workshop on Multimedia and Security, MM&Sec'11*, New York, NY, USA, pp. 9-14, 2011.

[44] B. Zhang, Y. Gao, S. Zhao, and J. Liu, "Local Derivative Pattern versus Local Binary Pattern: Face recognition with high-order local pattern descriptor," *IEEE Trans. Image Process.*, vol. 19, no. 2, pp. 533-544, Feb. 2010.

[45] T. Ojala, M. Pietikäinen, and T. Mäenpää, "Multiresolution gray-scale and rotation invariant texture classification with local binary patterns," *IEEE Trans. Pattern Anal. Mach. Intell.*, vol. 24, no. 7, pp. 971-987, 2002.

[46] C. C. Chang and C. J. Lin, "LIBSVM: A library for support vector machines," *ACM Trans. on Intell. Syst. and Technol.*, vol.2, pp. 27:1-27:27, 2011.

[47] G. Schaefer and M. Stich, "UCID-An uncompressed colour image database," *Storage and Retrieval Methods and Applications for Multimedia 2004*, SPIE Proc., vol. 5307 of, pp. 472-480, 2004.

[48] I. Sobel, "An isotropic 3×3 gradient operator," *Mach. Vision for Three-Dimensional Scenes*, Freeman, H., Academic Pres., NY, pp. 376-379, 1990.

[49] T. Pevny, P. Bas, and J. Fridrich, "Steganalysis by subtractive pixel adjacency matrix," *IEEE Trans. Inf. Forensics Security*, vol. 5, no. 2, pp. 215-224, 2010.

[50] I. Guyon, J. Weston, S. Barnhill, and V. Vapnik, "Gene selection for cancer classification using support vector machines," *Mach. Learning*, vol. 46, pp. 389-422, 2002.

[51] Y. LeCun, "Generalization and network design strategies," *Proc. Connectionism in Perspective*, Zurich, Switzerland, Oct. 1989.

[52] S. Becker and Y. LeCun, "Improving the convergence of back-propagation learning with second-order methods," *Proc. Connectionist Models Summer School*, Morgan Kaufman, San Mateo, pp. 29-37, 1988,

[53] Y. LeCun, B. Boser, J. S. Denker, D. Henderson, R. E. Howard, W. Hubbard, and L. D. Jackel, "Backpropagation applied to handwritten zip code recognition," *Neural Computation*, vol. 1, no. 4, pp. 541-551, 1989.

[54] Y. LeCun, L. Bottou, Y. Bengio, and P. Haffner, "Gradient-Based learning applied to document recognition," *Proc. IEEE*, vol. 86, no. 11, pp. 2278-2324, 1998.

[55] A. Krizhevsky, I. Sutskever, and G. Hinton, "Imagenet classification with deep convolutional neural networks," *Proc. Adv. Neural Inf. Process. Syst.*, pp. 1106-1114, 2012.

[56] O. Russakovsky, "ImageNet large scale visual recognition challenge," *Int. J. Comput. Vision*, vol. 115, pp. 211-252, 2015.

[57] M. D. Zeiler and R. Fergus, "Visualizing and understanding convolutional networks," *European Conf. Comput. Vision*, Springer International Publishing, 2014.

[58] K. Simonyan and A. Zisserman, "Very deep convolutional networks for large-scale image recognition," arXiv preprint arXiv:1409.1556, 2014.

[59] C. Szegedy, W. Liu, Y. Jia, P. Sermanet, S. Reed, D. Anguelov, D. Erhan, V. Vanhoucke, and A. Rabinovich, "Going deeper with convolutions," *Proc. IEEE Int. Conf. Comput. Vision Pattern Recog.*, pp. 1-9, Jun. 2015.

[60] K. He, X. Zhang, S. Ren, and J. Sun, "Deep residual learning for image recognition," *Proc. IEEE Conf. Comput. Vision Pattern Recog.*, 2016.

[61] Y. Qian, J. Dong, W. Wang, and T. Tan, "Deep learning for steganalysis via convolutional neural networks," *Proc. SPIE Media Watermarking Security Forensics*, vol. 9409, pp. 94090J-94090J-10, 2015.

[62] L. Pibre, J. Pasquet, D. Ienco, and M. Chaumont, "Deep learning is a good steganalysis tool when embedding key is reused for different images even if there is a cover source mismatch," *Proc. SPIE*, pp. 14-18, Feb. 2016.

[63] G. Xu, H. Wu, and Y. Q. Shi, "Structural design of convolutional neural networks for steganalysis," *IEEE Signal Process. Lett.*, vol. 23, Issue 5, pp. 708-712, 2016.

[64] S. Ioffe and C. Szegedy, "Batch normalization: accelerating deep network training by reducing internal covariate shift," *Proc. 32nd Int. Conf. Mach. Learning*, vol. 37, 2015.

[65] X. Glorot, A. Bordes, and Y. Bengio, "Deep sparse rectifier neural networks", *Proc. 14th Int. Conf. Artificial Intelligence Statistics*, 2011.

[66] P. Bas, T. Filler, and T. Pevný, "Break our steganographic system - the ins and outs of organizing BOSS," *Inf. Hiding, 13th Int. Conf.*, vol. 6958, LNCS, Prague, Czech Republic, pp. 59-70, May 18-20, 2011.

[67] Y. Jia, "Caffe: convolutional architecture for fast feature embedding," *Proc. ACM Int. Conf. Multimedia*, pp. 675-678, 2014.